SANDIA REPORT
SAND2013-8440
Unlimited Release
September 2013

Hybrid Models for the Simulation of Microstructural Evolution Influenced by Coupled, Multiple Physical Processes

Veena Tikare, Eric R. Homer, Efraín Hernández–Rivera, Jonathan D. Madison, Elizabeth A. Holm, Burton R. Patterson

Prepared by
Sandia National Laboratories
Albuquerque, New Mexico 87185

Sandia National Laboratories is a multi-program laboratory managed and operated by Sandia Corporation, a wholly owned subsidiary of Lockheed Martin Corporation, for the U.S. Department of Energy's National Nuclear Security Administration under contract DE-AC04-94AL85000.

Approved for public release; further dissemination unlimited.

Sandia National Laboratories

Issued by Sandia National Laboratories, operated for the United States Department of Energy by Sandia Corporation.

NOTICE: This report was prepared as an account of work sponsored by an agency of the United States Government. Neither the United States Government, nor any agency thereof, nor any of their employees, nor any of their contractors, subcontractors, or their employees, make any warranty, express or implied, or assume any legal liability or responsibility for the accuracy, completeness, or usefulness of any information, apparatus, product, or process disclosed, or represent that its use would not infringe privately owned rights. Reference herein to any specific commercial product, process, or service by trade name, trademark, manufacturer, or otherwise, does not necessarily constitute or imply its endorsement, recommendation, or favoring by the United States Government, any agency thereof, or any of their contractors or subcontractors. The views and opinions expressed herein do not necessarily state or reflect those of the United States Government, any agency thereof, or any of their contractors.

Printed in the United States of America. This report has been reproduced directly from the best available copy.

Available to DOE and DOE contractors from
U.S. Department of Energy
Office of Scientific and Technical Information
P.O. Box 62
Oak Ridge, TN 37831

Telephone: (865) 576-8401
Facsimile: (865) 576-5728
E-Mail: reports@adonis.osti.gov
Online ordering: http://www.osti.gov/bridge

Available to the public from
U.S. Department of Commerce
National Technical Information Service
5285 Port Royal Rd.
Springfield, VA 22161

Telephone: (800) 553-6847
Facsimile: (703) 605-6900
E-Mail: orders@ntis.fedworld.gov
Online order: http://www.ntis.gov/help/ordermethods.asp?loc=7-4-0#online

SAND2013-8440
Unlimited Release
September 2013

Hybrid Models for the Simulation of Microstructural Evolution Influenced by Coupled, Multiple Physical Processes

Veena Tikare and Efraín Hernández–Rivera
Storage & Transportation Technology
Sandia National Laboratories
PO Box 5800
Albuquerque, NM 87185-0779

Jonathan D. Madison
Comp Materials & Data Science
Sandia National Laboratories
PO Box 5800
Albuquerque, NM 87185-1411

Elizabeth A. Holm, Ph.D.
Professor, Materials Science and Engineering
Carnegie Mellon University
5000 Forbes Avenue
Wean Hall 3301
Pittsburgh, PA 15213

Burton R. Patterson
Department of Materials Science and Engineering
University of Florida
PO Box 116400
223 Materials Engineering Bldg. (MAE)
Gainesville, FL 32611-6400

Eric R. Homer
Brigham Young University
Dept. of Mechanical Engineering
435 CTB
Provo, Utah 84602

ABSTRACT

Most materials microstructural evolution processes progress with multiple processes occurring simultaneously. In this work, we have concentrated on the processes that are active in nuclear materials, in particular, nuclear fuels. These processes are coarsening, nucleation, differential diffusion, phase transformation, radiation-induced defect formation and swelling, often with temperature gradients present. All these couple and contribute to evolution that is unique to nuclear fuels and materials. Hybrid model that combines elements from the Potts Monte Carlo, phase-field models and others have been developed to address these multiple physical processes. These models are described and applied to several processes in this report. An important feature of the models developed are that they are coded as applications within SPPARKS, a Sandia-developed framework for simulation at the mesoscale of microstructural evolution processes by kinetic Monte Carlo methods. This makes these codes readily accessible and adaptable for future applications.

CONTENTS

ABSTRACT 4
CONTENTS 5
FIGURES 6
NOMENCLATURE 8
1. INTRODUCTION 9
   1.1 Current Models 11
2. HYBRID POTTS-PHASE FIELD MODEL FOR SIMULATOIN OF COUPLED GRAIN GROTH AND DIFFUSION IN A TWO-COMPONENT, TWO-PHASE SYSTEM 14
3. HYBRID POTTS-CELLULAR AUTOMATON MODEL FOR SIMULATOIN OF DYNAMIC RECRYSTALLIZATION 16
4. HYBRID POTTS-PHASE FIELD MODEL SIMULATION OF COUPLED MICROSTRUCTURAL COMPOSITIONAL EVOLUTION FOR SI-AL INFORMED BY THERMODYNAMIC DATABASE 18
5. SIMULATION OF RADIATION-INDUCED EGREGATION BY THE HYBRID POTTS-PHASE FIELD MODEL 20
   5.1 Evolution using Cahn-Hilliard Equation for Composition Evolution 20
      5.1.1 Model Development 20
      5.1.2 Results and Discussion 25
      5.1.3 Summary 26
   5.2 Hybrid Model with Chemical Potential Driving Composition Evolution 27
      5.2.1 Chemical Potential Definition 27
      5.2.2 Results and Discussion 28
      5.2.3 Summary 30
6. HYBRID POTTS-PHASE FIELD MODEL FOR COMPONENT SEGREGATION AND PHASE TRANSFORMATION IN U-PU-ZR FUELS 32
   6.1 Introduction 32
      6.1.1 Background 32
   6.2 Methodology 34
   6.3 Preliminary Results 36
7. DEVELOPMENT AND APPLICATION OF TOPOLOGICAL CHARACTERIZATION OF MICROSTRUCTURAL EVOLUTION 38
8. A MOVING MESH PHASE-FIELD MODEL FOR MICROSTRUCTURAL EVOLUTION 42
   8.1 Introduction 42
   8.2 Theory 43
      8.2.1 Description of the Computational Mesh and Its Movement 43
      8.2.2 Microstructural Evolution 43
   8.3 Results 44

FIGURES

Figure 1. Component segregation in U-Pu-Zr metallic fuel accompanied by regions of very different microstructural evolution[1]. 10

Figure 2. Dynamic recrystallization at the outer rim of fuels containing ^{238}U leads to nano-sized grains only at the rim as shown above[2]. 10

Figure 3. Accompanying the recrystallization in 2 are changes in porosity and Xe distribution in the rim[2]. Simulating recrystallization, pores reconfiguration with fission gas retribution will require a coupled microstructure-composition evolution model. 10

Figure .4 (a) Thermo-Calc phase diagram and (b) phase fraction resulting from simulations of the Al-Si system. Each is colored according to the triangular legend to illustrate the phase fractions at a given temperature and composition. 18

Figure 5: Isothermal chemical free energy curves for the two-component, four-phase system being modeled. 24

Figure 6: Vacancy concentration profile as it evolves with irradiation time. 25

Figure 7: Chemical composition profile as it evolves with irradiation time. 25

Figure 8: Evolution of the compositional and phase fields as the material is irradiated from the top. The creation and diffusion of the vacancies leads to chemical segregation and phase transformations. 27

Figure 9. Graphical representation of the chemical potential as defined by the Method of Intercepts–Common Tangent Construction approach. 28

Figure 10: Evolution of the chemical and vacancy compositional, and phase fields as the material with a distribution peaking at the center. The creation and diffusion of the vacancies leads to chemical segregation and phase transformations; where red is the AB phase, blue is the α phase and white is the β phase. 29

Figure 11: Chemical and vacancy concentration distribution along two different paths (inserts). We look at the concentration evolution along paths that include: a. nucleation of two phases, α and β. and b. nucleation of a single phase, α, ... 30

Figure 12. Micrograph of a U-Pu-Zr alloy, post-irradiation. Note the significant constituent redistribution driving the resulting concentric zones in the microstructure[8]. 33

Figure 13. Phase diagram for the U-Pu-Zr system at 933 and 868 K, curtsey of Kurata. 35

Figure 14. Simulation of U-25Zr-15Pu showing grain growth, phase nucleation and growth, phase and component segregation and evolving temperature profile. 36

Figure 15. Steele's Schlegel tree illustrating grain forms in face classes 4 through 8. Solid arrows indicate paths of downward transition to the end state of a tetrahedron due to loss of particular 3-edged faces by Type I or III events. Dashed arrows indicate horizontal transitions within the face class, due to neighboring grains participating in Type II or III events. 39

Figure 16. Contact affinity between grain pairs (a) of different face classes and (b) as a function of the product of face curvatures of the contacting grains..... 40

Figure 17. Simulation of grain growth using the moving mesh phase field model. 45

Figure 18. Simulation of grain growth in a thin film with large grains traversing the periodic boundary conditions in the x-direction. The distortion in the mesh do not distort the overall grain structure. 45

NOMENCLATURE

2D	two-dimensional
3D	three-dimensional
CA	Cellular Automaton
LLW	Low-Level Waste
NE	Nuclear Energy
MC	Monte Carlo
MCS	Monte Carlo Step
MMF	mesh monitor function
NSF	National Science Foundation
RIS	Radiation-Induced Segregation

1. INTRODUCTION

The formation, transport and segregation of components in nuclear fuels fundamentally control their behavior, performance, longevity and safety. Most nuclear fuels enter service with a uniform composition consisting of a single phase with two or three components. Fission products form introducing more components. The segregation and transport of the components is complicated by the underlying microstructure consisting of grains, pores, bubbles and more, which is evolving during service. As they evolve, components and microstructural features interact such that composition affects microstructure and vice versa. The ability to predict compositional and microstructural evolution in 3D as a function of burn-up would greatly improve the ability to design safe, high burn-up nuclear fuels.

This same ability to couple microstructural and compositional evolution would greatly benefit other nuclear materials and a wide range of other materials technologies as well. Claddings for nuclear fuels undergo a complex phase transformation involving the nucleation and growth of hydride precipitates; core materials undergo radiation-induced component segregation; diffusive phase-transformations are ubiquitous in many technologies; joining of components often involves dissimilar materials with coupled compositional and microstructural evolution. All of these materials technologies would benefit from the models developed in this project.

Simulations of the coupled multiple processes was achieved by developing models that combine existing models. Well-developed models exist for simulating microstructural evolution by processes such as grain growth, recrystallization, Ostwald ripening and sintering as well as for compositional evolution by diffusion, segregation and phase transformation. However, models coupling the two have been lagging. This coupling would enable simulation and prediction of processes such as component segregation in metal fuels[1] (shown in Figure 1), dynamic recrystallization and fission product distribution in low-level waste reactor (LWR) fuels as a function of radial distance and in the rim region[2] (shown in Figures 2 & 3), chemical interaction between the fuel and clad, restructuring of fast reactor fuels and many other microstructural-compositional evolution seen in all types of NE fuels. In all these processes, the compositional and microstructural evolution are coupled, meaning that the evolution of one influences the other and therefore must be captured in the same model. Treating them as separate and parallel processes does not capture its interdependence and therefore cannot be predictive. The composition, microstructure and their evolution during service controls the engineering performance, safety and longevity of fuels during normal and off-normal operation and post-service storage. Thus controlling and predicting such behavior is important.

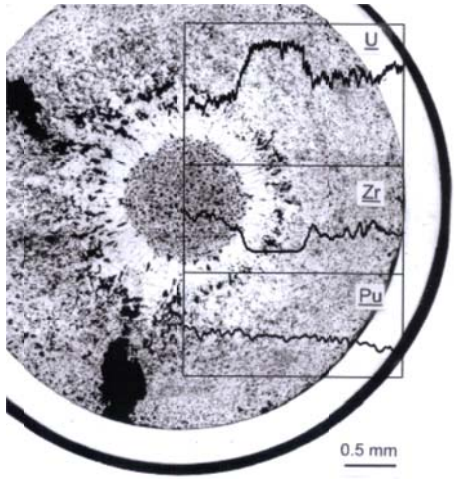

Figure 1. Component segregation in U-Pu-Zr metallic fuel accompanied by regions of very different microstructural evolution[1].

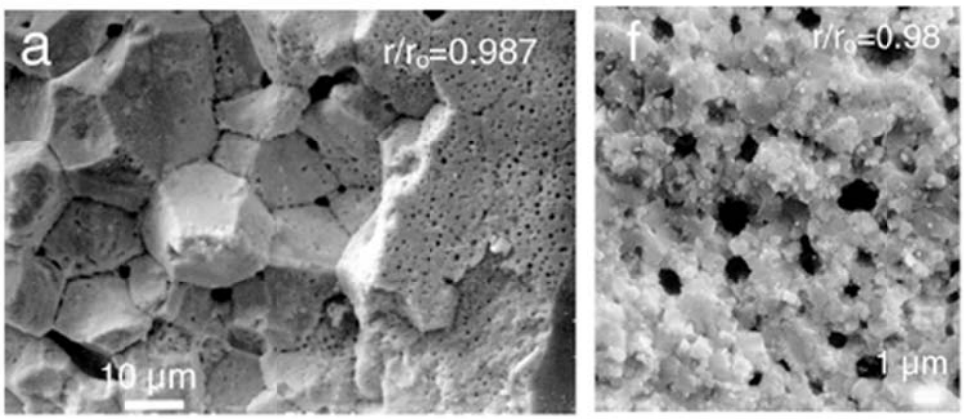

Figure 2. Dynamic recrystallization at the outer rim of fuels containing ^{238}U leads to nano-sized grains only at the rim as shown above[2].

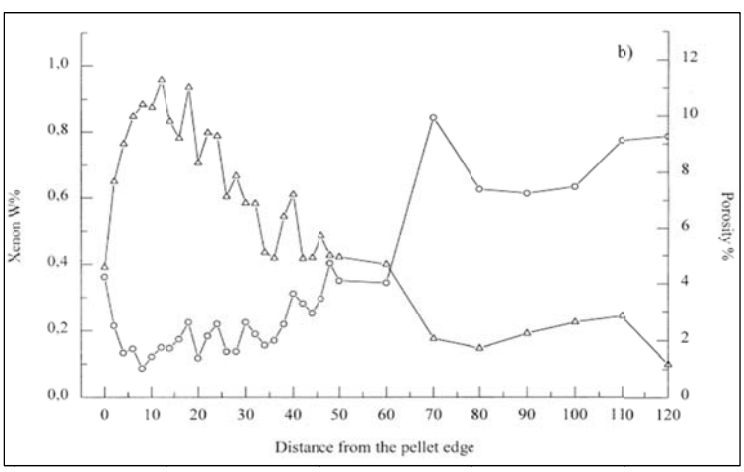

Figure 3. Accompanying the recrystallization in 2 are changes in porosity and Xe distribution in the rim[2]. Simulating recrystallization, pores reconfiguration with fission gas retribution will require a coupled microstructure-composition evolution model.

1.1 Current Models

The two dominant models currently used for microstructural models are the Potts Monte Carlo (MC) method and the phase-field model. Potts MC is a statistical-mechanical model that populates a lattice with an ensemble of discrete particles to represent and evolve the microstructure. The particles evolve in a variety of ways to simulate microstructural changes. Potts MC methods have proven themselves to be versatile, robust and capable of simulating various microstructural evolution processes. They have the great advantage of being simple and intuitive, while still being a rigorous method that can incorporate all the thermodynamic, kinetic and topological characteristics to simulate complex processes. They are easy to code, readily extendable from two-dimensional (2D) to three-dimensional (3D) and can simulate the underlying physics of many materials evolution processes based on the statistical-mechanical nature of the model. These processes include curvature-driven grain growth[1,2], anisotropic grain growth[3], recrystallization[4], grain growth in the presence of a pinning phase[5,6], Ostwald ripening[7,8], and particle sintering[9,10,11,12]. The equation of state characterizing the materials in Potts MC is the sum of the bulk energy of each particle at each site i and the sum of all the interfacial energy of each particle as

$$E_{MC} = \sum_{i=1}^{N} \left(E_v(q_i) + \frac{1}{2} \sum_{j=1}^{n} J(q_i, q_j) \right) \tag{1}$$

where N is the total number of particles, E_v is the bulk energy the particle at site i, J is the neighbor interaction energy of particle at site i with its neighbor j for a total number of neighbors n and q_i is the grain orientation and or phase of particle at site i. Highly tailored equations of state for many different types of materials processes can be constructed using this basic equation.

In contrast, the phase-field model is a deterministic, continuum, thermodynamic model that describes the microstructure and its evolution in terms of continuum "phase-fields" that are evolving. The phase-fields can be grain orientations, composition, phases or other microstructural and compositional descriptors. While phase-fields are continuum quantities, their evolution is simulated by solving their field equations on some predefined grid, typically square in 2D and cubic in 3D. The size of the grid is such that the distance between solution points is much larger than atoms, but sufficiently small to resolve microstructural features such as grain boundaries. The phase-field method is a powerful mesoscale modeling method that is widely used to model the kinetics of microstructural evolution in materials. The appeal of the phase-field method is that it uses directly constructed free energy functionals as functions of the "phase-fields" to describe their thermodynamics (equation of state) and use the time-dependent Ginzburg-Landau equation to treat the evolution of the non-conserved phase-fields and the Cahn-Hilliard equation for conserved phase-fields. The phase field model has been used extensively to simulate many microstructural evolution processes including grain growth[13] and Ostwald ripening[14], gas bubbles in nuclear fuels[15,16], void ensembles under irradiation[17], precipitate morphology and evolution in alloys[18], nucleation and growth near a dislocation[19], coarsening of precipitates[20] and solidification[21,22]. The phase-field equation of state is a sum of the bulk energy and interfacial energies as a function of all Q phase-fields η_i integrated over the simulation volume V as

$$E_{pf} = \int \left(f_o + \sum_{i=1}^{Q} \kappa_{\eta i} (\nabla \eta_i)^2 \right) dV \tag{2}$$

where f_o is the bulk free energy and is a function of all the phase fields Q and their interaction with each other. An example of a free energy functional used for grain growth is

$$f_o = \sum_{i=1}^{Q} \left(-\alpha \eta_i^2 + \beta \eta_i^4 \right) + \gamma \sum_{i=1}^{Q} \sum_{j \neq i}^{Q} \eta_i^2 \eta_j^2 \tag{3}$$

where α, β, γ are phenomenological constants used to obtain the desired thermodynamics. The second term with $\kappa(\nabla \eta_i)$ is the interfacial energy term where is a phenomenological constant used to define the energy and width of the interface. Like the Potts MC model, highly tailored equations of state for many different types of materials processes can be constructed using this basic equation.

However, both models do have drawbacks. Since, the Potts MC model uses an ensemble of particles to represent microstructure, smoothly varying compositions such as those required for the examples given in Figures 1 and 2 are difficult to represent and require very large simulations. Furthermore, diffusive transport has been simulated by random walk of particles; again requiring large ensembles for accurately sampling gradients in composition. Phase-field models are able to represent compositional gradients overlaying microstructural features well by using different phase-fields, but construction of the free energy functionals E_{pf} for coupling these phase-fields is very difficult and introduction of each set of couple phase-fields reduces the time and spatial increments to resolve them. Thus, simulations with coupled phase-fields become very time consuming to develop the free energy functionals and very computationally intensive, requiring massively parallel simulations. Almost all phase-field simulations published in the literature apply the technique to small 2D simulations to demonstrate the technique rather than to production-scale materials process simulation that can be used to study mesoscale materials behavior.

In addition to the Potts MC and phase-field models, others models were incorporated into the different hybrid methods as necessary to simulate behaviors such as nucleation and irradiation defect energy incorporation. These models will be described in the sections of the report that address the specific models and applications individually.

---

[1] M. P. Anderson, D. J. Srolovitz, G. S. Grest, and P. S. Sahni, "Computer-simulation of grain-growth. 1. Kinetics" *Acta Metall*., 1984, 32, 783-791.
[2] E. A. Holm, J. A. Glazier, D. J. Srolovitz, G. S. Grest, "Effects of lattice anisotropy and temperature on domain growth in the 2-dimenstional Potts-model", *Phys. Rev. A*, 1991, 43, 2662-2668.
[3] E. A. Holm, G. N. Hassold and M. A. Miodownik, "On misorientation distribution evolution during anisotropic grain growth", *Acta Mater*., 2001, 49, 2981-2991.
[4] E. A. Holm, M. A. Miodownik and A. D. Rollett, "On abnormal subgrain growth and the origin of recrystallization nuclei, *Acta Mater*., 2003, 51, 2701-2716.

[5] M. Miodownik, J.W. Martin and A. Cerezo, "Mesoscale simulations of particle pinning," *Phil. Mag. A*, 1999, 79, 203-222.
[6] V. Tikare, M. Miodownik, E. A. Holm, "Three Dimensional Simulation of Grain Growth in the Presence of Mobile Pores," *J. Am. Ceram. Soc*., 2001, 84, 1379-1385.
[7] V. Tikare and J.D. Cawley, "Numerical Simulation of Grain Growth in Liquid Phase Sintered Materials – I. Model," *Acta Mater*. 1998, 46 1333-1342.
[8] V. Tikare and J. D. Cawley, "Numerical Simulation of Grain Growth in Liquid Phase Sintered Materials – II. Study of Isotropic Grain Growth," *Acta Mater*., 1998, 46, 1343-1356.
[9] G.N. Hassold, I-W. Chen, D. J. Srolovitz, *J. Am. Ceram. Soc.*, 1990, 73, 2857-2864.
[10] M. Braginsky, V. Tikare and E. Olevsky, "Numerical Simulation of Solid State Sintering," *Int. J. Sol. Struc.*, 2004, 42, 621-636.
[11] V. Tikare, M. Braginsky and E.A. Olevsky, "Numerical Simulation of Solid-State Sintering: I, Sintering of Three Particles," *J. Am. Ceram. Soc*., 2003, 86, 49-53.
[12] V. Tikare, M. Braginsky, D. Bouvard and A. Vagnon, "Numerical Simulation of Microstructural Evolution during Sintering at the Mesoscale in a 3D Powder Compact," *Comp. Mat. Sci.*, 2010, 48, 317-325.
[13] D. Fan and L. Q. Chen, "Computer simulation of grain growth using a continuum field model," *Acta Materialia*, 1997. 45 611-622.
[14] V. Tikare, E.A. Holm, D. Fan and L.Q. Chen, "Comparison of Phase-Field and Potts Models for Coarsening Processes" *Acta Mater*. 47 363-371 (1999).
[15] S. Y. Hu, C. H. Henager Jr., H. L. Heinisch, M. Stan, M. I. Baskes and S. M. Valone, "Phase-field modeling of gas bubbles and thermal conductivity evolution in nuclear fuels," *J. Nucl. Mater.*, 2009, 392, 292-300.
[16] S. Y. Hu, Y. L. Li, X. Sun, F. Gao, R. Devanathan, C. H. Henager Jr. and M. Khaleel, "Application of the phase-field method in predicting gas bubble microstructure evolution in nuclear fuels," *Intl. J. Mater. Res.*, 2010, 101 (4), 515-522.
[17] S. Y. Hu and C. H. Henager Jr., "Phase-field modeling of void lattice formation under irradiation," *J. Nucl. Mater.*, 2009, 394, 155-159.
[18] S. Y. Hu and C. H. Henager Jr., "Phase-field simulations of Te-precipitate morphology and evolution kinetics in Te-rich CdTe crystals," *J. Crystal Growth*, 2009, 311, 3184-3194.
[19] S. Y. Hu and L. Q. Chen, "Solute segregation and coherent nucleation and growth near a dislocation - A phase-field model integrating defect and phase microstructures," *Acta Mater*., 2001, 49, 463-472.
[20] V. Vaithyanathan and L. Q. Chen, "Coarsening of ordered intermetallic precipitates with coherency stress," *Acta Mater.*, 2002, 50, 4061-4073.
[21] W. J. Boettinger, J. A.Warren, C. Beckermann, and A. Karma, "Phase-field simulation of solidification," *Annu. Rev. Mater. Res*.,2002, 32, 163-194.
[22] L. Q. Chen, "Phase-field models for microstructure evolution," *Annu. Rev. Mater. Res* , 2002, 32, 113-140.

2. HYBRID POTTS-PHASE FIELD MODEL FOR SIMULATOIN OF COUPLED GRAIN GROWTH AND DIFFUSION IN A TWO-COMPONENT, TWO-PHASE SYSTEM

Microstructural evolution cannot be decoupled from compositional evolution in alloyed materials. This is especially true for the evolution of multi-phase materials or for phase transformations in materials that are limited by diffusion kinetics. This coupling results from the fact that the local microstructure, which is often expressed only in terms of grains, grain boundaries, orientations, etc., is actually defined in part by the local composition. Furthermore, these microstructural and compositional fields are strongly influenced by a number of thermal and thermo-mechanical environments that induce driving forces for their evolution. Understanding the coupling between microstructure, composition, and environment is critical to modeling materials processing and performance in conventional alloys systems as well as in extreme environments such as those experienced by nuclear materials.

A model that can treat grain growth with diffusion was developed. It can simulate evolution in a two component system with two-phases. In such a system, the grain growth is driven by the reduction in the overall interfacial energy by coarsening while maintaining the minimum energy composition for the two phases independently of each other. This model has been described in detail in previously published work; there it will only be summarized here. The reader is directed to Homer, Tikare and Holm[1] for a comprehensive description. A hybrid Potts-phase-field model was introduced, described and demonstrated. It combines elements of the Monte Carlo Potts Model with those of the phase field model. This hybrid model is introduced as a method to simulate microstructural evolution processes that are kinetically controlled by long-range diffusion in multi-component systems. The hybrid model uses a digitized microstructure with each site characterized by its microstructural features and its composition. The total free energy of the system is defined by bulk chemical free energy as well as interfacial energy. The coupling between the microstructure and composition is achieved by using the total free energy to drive the evolution in both fields. The kinetics are simulated by a combination of Monte Carlo methods and solution of the Cahn–Hilliard equation. This model is applied to several example problems to demonstrate its capabilities. These are diffusion in single- and two-phase diffusion couples, grain growth in a two-phase system controlled by diffusion and diffusion phase transformation by nucleation and growth of a second phase.

The new hybrid Monte Carlo Potts-phase field model has the capability to simulate the coupled evolution of microstructure and composition. The model is efficient because the microstructure is modeled by Monte Carlo Potts methods while the composition is modeled by the phase field method. The coupling between the microstructure and composition occurs through a free energy functional that can be extended and modified to capture different phenomena and processes. The framework has been incorporated into the open-source SPPARKS framework, maintained by Sandia National Laboratories. The hybrid modeling framework applied to a simple two-phase, two-component system has been shown to capture

- Grain growth and phase coarsening

- Coupling between phase and composition
- Fickian diffusion of the two components
- Diffusion-limited grain growth
- Phase transformations to a second phase by nucleation and growth of the stable phase from a super-saturated single-phase

The hybrid Potts-phase field modeling framework is efficient, versatile and easily extensible to incorporate different phenomena. Such a model is expected to have a significant impact on the ability to simulate real materials behaviors where the microstructural and compositional evolution cannot be decoupled.

---

[1] E.R. Homer, V. Tikare, E.A. Holm, "Hybrid Potts-Phase Field Model for Coupled Microstructural-Compositional Evolution," *Comp. Mater. Sci.*, 69 414–423 (2013).

3. HYBRID POTTS-CELLULAR AUTOMATON MODEL FOR SIMULATION OF DYNAMIC RECRYSTALLIZATION

Recrystallization is a process by which low free energy, damage free material nucleates and grows to replace high free energy, damaged material. Thus, the driving force for recrystallization is the excess free energy associated with the damage to the crystalline grains, whether by dislocations, vacancies, or other irradiation induced defects, and the rate of recrystallization increases with the amount of damage. In typical metallurgical systems, plastic deformation supplies damage in the form of dislocations. During recrystallization, dislocation-free grains nucleate and consume the damaged matrix. The final structure is free of dislocations and typically has properties (grain size, hardness, ductility) different from the initial damaged system.

In nuclear fuels, the rim region is a prime candidate for recrystallization due to its enhanced damage accumulation, which arises from two causes. First, with increased enrichment at high burn-up, it is estimated that fission events occur in the rim at a rate 2–3 times that of the bulk leading to a higher rate of damage formation. Second, the temperature in this rim region is the lowest in the fuel with a homologous temperature $T/T_m \approx 0.2$, where T_m is the melting temperature. At this low temperature, the diffusive mechanisms available to heal damage occur very slowly; thus, damage can accumulate to critical levels.

High burn-up, rim structures within uranium dioxide (UO_2) light water reactor fuels exhibit marked differences in microstructure that are attributed to dynamic recrystallization. The recrystallization process has three distinct, interacting components: damage accumulation, nucleation and growth of damage-free regions, and subsequent evolution of recrystallized grains. The microstructural-scale simulation techniques for all three processes are presented and assembled into a hybrid tool for modeling the entire dynamic recrystallization process. This hybrid model is described in great detail in previously published work and will not be reiterated here. Only a summary of the model is presented in this report and the reader is directed to Madison, Tikare and Holm[1] for the complete work. The components of the model include a phenomenological model for damage accumulation and nucleation, a Cellular Automaton (CA) model for the growth and impingement of recrystallized grains, and a Monte Carlo Potts model for subsequent grain growth.

A model that can incorporate all the physical phenomena necessary to simulate dynamic recrystallization observed in the outer rim of high-burnup LWR fuels has been presented. The kinetic rates for grain boundary mobility driven by curvature and by recrystallization can be varied relative to one another. Additionally, the nucleation conditions can also be varied to control the activation energy required for nucleation, by setting a threshold energy factor, g, and nucleation rate factor, η. These simulation parameters can be selected to match the varied conditions of different fuels and reactors to develop understanding and predictive capabilities for advanced fuel design or investigation of high-burnup conditions.

[1] J. Madison, V. Tikare and E.A. Holm, "A hybrid simulation methodology for modeling dynamic recrystallization in UO2 LWR nuclear fuels," *J. Nucl. Mater.*, 425 173-180 (2012).

4. HYBRID POTTS-PHASE FIELD MODEL SIMULATION OF COUPLED MICROSTRUCTURAL-COMPOSITIONAL EVOLUTION FOR SI-AL INFORMED BY THERMODYNAMIC DATABASE

In previous work discussed in Section 2, the hybrid Potts-phase field model was shown to be an effective and efficient method to simulate coupled grain growth and compositional evolution in an idealized two-component, two-phase system. In this work, the same model is extended to simulate a real materials system, Al-Si binary system with three phases, using thermodynamic data calculated by Thermo-Calc. This method is described in previously published work by Cox, Homer and Tikare[1] and will be summarized here.

The hybrid model requires accurate free energy functionals to correctly represent material behavior. This task grows more challenging when considering multi-component and multi-phase systems, which are common in today's alloys. The purpose of this paper is to incorporate readily available thermodynamic databases, which represent the free energy functions of an binary system, into the hybrid Potts-phase field model. In this work, the Si-Al binary is chosen as the thermodynamic data is readily available. The new framework incorporates thermal diffusion into the model and is readily extendable to multicomponent systems, allowing alloys with any number of component or phases to be modeled. The application of the framework to the Al-Si system is demonstrated with validation calculations showing good agreement between a calculated phase diagram obtained from the hybrid simulations and an experimentally obtained one.

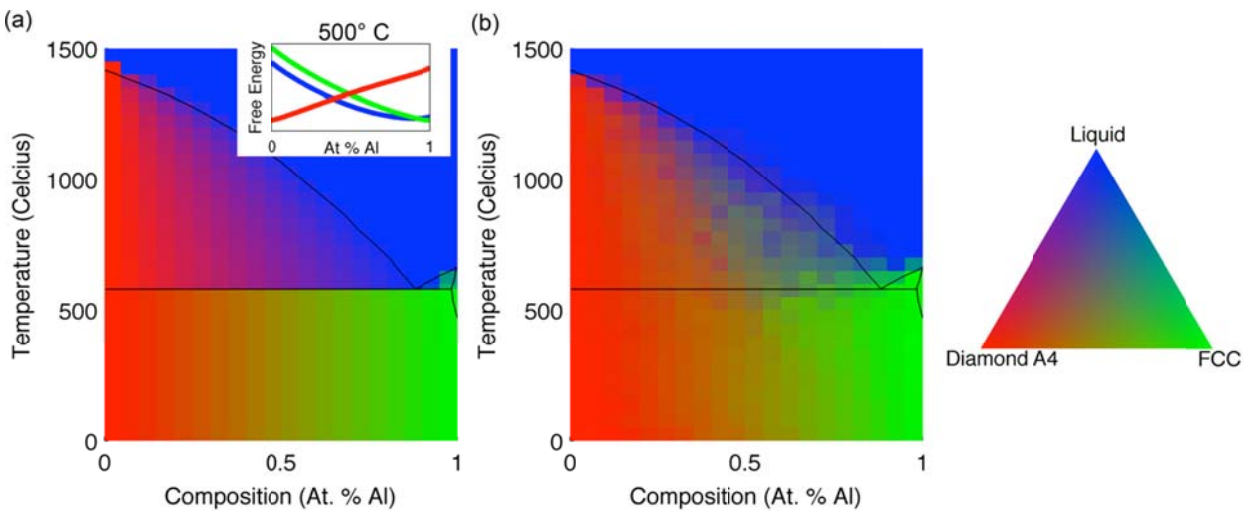

Figure .4 (a) Thermo-Calc phase diagram and (b) phase fraction resulting from simulations of the Al-Si system. Each is colored according to the triangular legend to illustrate the phase fractions at a given temperature and composition.

The thermodynamic data for the Al-Si system is obtained from Thermo-Calc software. Six hundred simulations were run with compositions varying from 0 to 1.0 fraction of Al and temperatures ranging from o to 1500 ^{o}C. The free energy functionals for the three phases of the Al-Si system were exported from Thermo-Calc and imported into the Potts-phase field application style that has been developed to work with the SPPARKS code. Figure 4(a) illustrates the phase diagram of Al-Si obtained from the Thermo-Calc software, with an inset of the free energy curves at 500° C. The phase diagram and inset have been overlaid with a color scheme to illustrate the expected phase fractions for a given composition and

temperature. The phase diagram calculated from the simulations shown in Figure 4(b) is in good agreement with the experimentally obtained phase diagram. Small fractions of liquid phase persist in the simulations, but generally good agreement is obtained. This work demonstrates the hybrid Potts-phase field model shows promising abilities to simulate coupled microstructural and compositional evolution with input from thermodynamic databases.

---

[1] J.J. Cox, E.R. Homer and V. Tikare, "Coupled microstructural-compositional evolution informed by a thermodynamic database using the hybrid Potts-phase field model," Mater. Res. Soc. Symp. Proc. Vol. 1524, DOI: http://dx.doi.org/10.1557/opl.2013.165.

5. SIMULATION OF RADIATION-INDUCED SEGREGATION BY THE HYBRID POTTS-PHASE FIELD MODEL

5.1 Evolution using Cahn-Hilliard Equation for Composition Evolution

Radiation events lead to the creation of over–saturated point defects, causing unique microstructural changes including radiation–induced segregation (RIS). It is well known that ion–irradiation can lead to chemical separation in a multi–component system, which is essentially an effect driven by the difference in diffusivities of interstitials and vacancies of the different components. This radiation effect has been observed in a wide variety of materials including binary[1,2] and multi–component[3] systems. Some of these materials also show interesting microstructural features forming like nano–cones[4] and nano–fibrous structures[5].

Diffusion in irradiated materials has been widely studied[6], mostly for metallic multi–component systems under in–reactor radiation conditions where the material is subjected to high ion energy fluxes. RIS has also been observed in materials subjected to low to mid ion energy irradiation. However, under these conditions, sputtering theory says that the apparent chemical segregation observed due to preferential sputtering of the different component near the surface region rather than differential diffusion. Sputtering theory has also been employed to explain the formation surface nano–structures[7], like nano–cones[4,8], nano–ripples[7,9] and quantum dots[10]. *Madi et al.*, propose another mechanism to explain the formation of these surface nano–structures; they suggested mass redistribution lead to nano–structure formation[11]. In this work, we pose the question, "Can differential diffusivities lead to RIS and associated phase transitions?" We use numerical simulations to study compositional evolution, phase transformation and microstructural changes of a binary system under irradiation.

5.1.1 Model Development

A binary (AB) system with thermodynamic characteristics of $GaAs$ is studied. However, since diffusion of defects in $GaAs$ is inherently complex leading to disagreement on diffusion data interpretation[12], we do not claim to simulate $GaAs$. A hybrid model that couples continuum and statistical methods is used to simulate the generation of defects due to irradiation, diffusion of components A and B, phase transformation and microstructural evolution. The model is based on the hybrid Potts–phase field model developed by *Homer et al.*[13], but is further developed to simulate radiation damage and its effects on diffusion.

5.1.1.1 Microstructural and Composition Representation

We use continuous fields to represent the chemical composition and vacancy density, and discrete fields to represent the phases. The simulation space is digitized into 2D squares, called sites, where the discrete field in each square describes its phase state and the continuous fields have digitial values at that grid point. The starting microstructure consists of an AB $(GaAs)$ solid in contact with vacuum, called void. The concentration of vacancies is zero (as the equilibrium vacancies is very low) and the chemical composition is $C_A = C_B = 0.5$ at all sites. Periodic boundary conditions are used in the x-direction only, hence, in effect, the solid is a semi–infinite solid with an irradiated surface in contact with a vacuum.

5.1.1.2 Radiation Damage

Radiation damage in the form of point defects is calculated by a two–step process. First, the number of defects created is calculated. Second, the number of defects that survive the quenching stage and contribute to microstructural evolution is calculated. A TRIM[14] simulation of a 30 keV Ga^+ −ion on a $GaAs$ target is used to determine the number of Frenkel pairs created per unit volume per unit time as a function of distance from the target surface, z. This defect density distribution is assumed to be directly proportional to the probability of a collision at a depth z from the surface. Using TRIM, the energy deposition distribution is obtained and is used to calculate the number of defects that have been created in each site i. The defect distribution obtained in this manner results is a simple Gaussian distribution

$$\Upsilon = \Upsilon_0 \cdot exp\left(-\left[\frac{z-\bar{z}}{\sigma}\right]^2\right) \tag{3}$$

where $\Upsilon(z)$ is the energy deposited at z–depth, Υ_0 is the distribution's "amplitude", $\bar{z}$ is the average depth at which the distribution peaks and σ is the standard deviation.

For clarity, let us "follow" an ion as it travels through the simulation space. As we iterate through each site in the simulation space, we compare the probability of collision (p_{coll}) at that site's depth z to a randomly generated number (RN) uniformly distributed between [0,1]. If $RN > p_{coll}$, we say that a collision occurred at the site. If a collision event occurred, the distribution of energy deposited is used to calculate how much energy was deposited in the site's volume. The amount of energy deposited is then used to calculate the number of point defects created in the collision cascade contained within the site's volume. Since the defects that survive the collision cascade after they quench are the ones that contribute to diffusion and RIS, we use the method employed by *Hobler et al.*[15] to calculate the number of *surviving* defects

$$\eta_s(E_T) = \eta_{TRIM}(E_T) f_{rec}\left(1 - 2p_{ref}\right) \tag{4}$$

where $\eta_{TRIM}(E_T)$ is the number of Frenkel pairs created due to the energy transferred (E_T) as calculated from TRIM, f_{rec} is the fraction of η_{TRIM} that did not recombine within the collision cascade and p_{rec} is the probability that a newly created defect will recombine with a pre−existing defect. We should note that for simplicity, we only consider the creation of vacancy defects. In this manner, the vacancy concentration at each site increases continuously throughout irradiation.

5.1.1.3 Chemical and Vacancy Evolution

The RIS model developed by *Wiedersich et al.* couples point defect kinetic equations to track the evolution of these defects. In this hybrid model, we model this field by use of an adapted Cahn–Hilliard equation

$$\frac{\partial C_v}{\partial t} = \eta_s(\Delta t) + \nabla \cdot \left(M_{C_v} \nabla \cdot \left[\frac{\partial f_v}{\partial C_v} - \kappa_{C_v} \nabla^2 C_v\right]\right) \tag{5}$$

where $\eta_s(\Delta t)$ is the additional concentration of surviving defects during irradiation time interval Δt, M_{C_v} is the mobility of the vacancies, κ_{C_v} is an interfacial energy constant and f_v is the vacancy bulk free energy defined as by the regular solution equation

$$f_v = \frac{1}{\Omega}\left(E_v^f C_v + k_B T[C_v ln(C_v) + (1 - C_v) ln(1 - C_v)]\right) \tag{6}$$

where Ω is the unit site volume and E_v^f is the vacancy formation energy.

For the evolution of the chemical components, we use an approach similar to the one given by *Wiedersich*[2], and outlined in *Was*[6]. The different point defect fluxes through an AB system are

$$\begin{aligned} J_i &= J_i^A + J_i^B \\ -J_v &= J_v^A + J_v^B \end{aligned} \tag{7}$$

where J_i^A is the flux of defect i through the site of A component. Since we are considering a binary system and using Fick's first law, Eq. 7 could be simplified for a single component

$$\mathrm{C_A} + \mathrm{C_B} = 1 \rightarrow \nabla \mathrm{C_A} = -\nabla \mathrm{C_B} \tag{8}$$

Now, using Fick's second law and setting the net flux to include diffusion due to chemical gradients and through the defect mechanisms just discussed, we have

$$\frac{\partial C_B}{\partial t} = \nabla \cdot (D_B \nabla C_B - D_v^B \nabla C_v + D_i^B \nabla C_i) \tag{9}$$

where the first term is the flux due to a chemical gradient, and the second and third terms are fluxes through the vacancy and interstitial defects, respectively. Since only the creation of vacancies is considered, the third term in the RHS of Eq. 9 is not included in our hybrid model. Lastly, we should point out that we assume that the B component diffuses faster than A through the vacancy mechanism, i.e., $D_A^v < D_B^v$

We use the standard approach for non–dimensionalizing the Cahn−Hilliard equation. We define a set of normalizing parameters to non−dimensionalize Eq. 5. The normalizing parameters are energy

$$E_n = k_B T \tag{10}$$

and length

$$l = \sqrt{\frac{\kappa_{C_v}}{k_B T}} \tag{11}$$

where interfacial energy constant, κ_{C_v}, has units of $length^2 \cdot energy$ giving l units of length. Finally, normalized time is

$$\tau = \frac{l^2}{D} = \frac{l^2}{M_{C_v} k_B T} \tag{12}$$

where the mobility, M_{C_v}, has units of $length^2/(energy \cdot time)$ g τ units of time. Eqs. 5 and 9 in their non–dimensional forms are obtained by applying to the corresponding quantities by normalized energy, length or time as

$$\frac{\partial C_v}{\partial \tilde{t}} = \tilde{\eta}_s(\Delta \tilde{t}) + \tilde{\nabla} \cdot \left(\widetilde{M}_{C_v} \tilde{\nabla} \cdot \left[\frac{\partial \tilde{f}_v}{\partial C_v} - \tilde{\kappa}_{C_v} \tilde{\nabla}^2 C_v\right]\right) \tag{13}$$

and

$$\frac{\partial C_B}{\partial \tilde{t}} = \tilde{\nabla} \cdot \left(\widetilde{D}_B \tilde{\nabla} C_B - \widetilde{D}_v^B \tilde{\nabla} C_v + \widetilde{D}_i^B \tilde{\nabla} C_i\right). \tag{14}$$

We should point out that the radiation damage equations were generated as to obtain distributions that yield an ion range of $\sim 30\ nm$. As for each pixel, we treat them as cubes of length $L \approx 2\ nm$.

5.1.1.4 Phase Transformations

We use a discrete integer value at each site to describe its phase state, which are: AB, A–rich, B–rich and liquid. These are defined by the free energy curves plotted in Figure 5. When a site's energy has been increased due to a collision event to that at or above another phase's energy, then the site's phase is changed to that higher energy phase.

Phase transitions can also occur by each site attempting to nucleate another phase. If the change in energy calculated by Eq. 15 lowers the chemical bulk free energy, f_A^{bulk}, the phase transition event occurs. These nuclei can grow and coalesce in a similar process by growing into the neighboring sites again with a transition probability given by Eq. 15.

$$P_{\text{phase change}} = \begin{cases} \text{change}, & \Delta f_A^{bulk} \leq 0 \\ \text{no change}, & \Delta f_A^{bulk} > 0 \end{cases} \tag{15}$$

where Δf_A^{bulk} is the difference between the chemical bulk free energy (Figure 5). For a phase nucleation event we compare the difference in the chemical bulk free energies of the different phases. If the new phase yields a lower free energy curve, then the phase change is accepted.

5.1.1.5 Surface Diffusion

In addition to the surface diffusion described in Section *Chemical and Vacancy Evolution*, surface diffusion is also simulated by exchanging mass and void sites at the surface as described in *Holm et al.*[16], and implemented by *Homer*. This leads to roughening of the material surface. The probability that an exchange will happen, is given by

$$P_{\text{surf mig}} = \begin{cases} 1, & \Delta E_{int} \leq 0 \\ exp\left(-\frac{\Delta E_{int}}{k_B T}\right), & \text{otherwise} \end{cases} \tag{16}$$

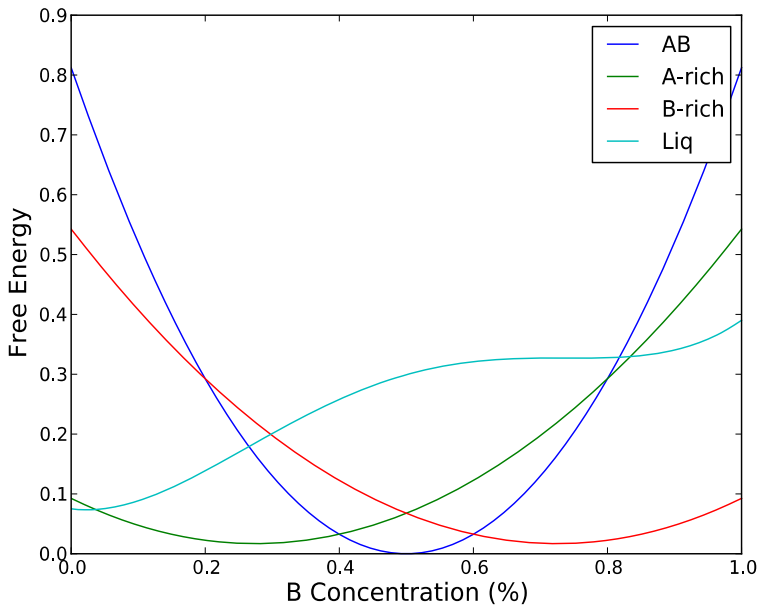

Figure 5: Isothermal chemical free energy curves for the two-component, four-phase system being modeled.

where ΔE_{int} is the difference between the interface energy for the i and j sites before and after the exchange

$$\Delta E_{int} = [E_{int}(\text{site } i) + E_{int}(\text{site } j)]_1 - [E_{int}(\text{site } i) + E_{int}(\text{site } j)]_0 \quad (17)$$

where E_{int} is the interface energy[13,16].

5.1.1.6 Processes Implementation

This hybrid model is able to incorporate all these processes to simultaneously simulate of the microstructural evolution due to ion irradiation. The simulation proceeds as

1. Calculate if a collision event occurs, i.e. $p_{coll} < RN$
   a) If $p_{coll} < RN$, calculate number of stable defects created and locally update the vacancy concentration, η
2. Attempt a surface diffusion event by site exchange, with frequency $\omega_{\text{surf mig}}$ $(= 0.2)$
3. For time iterations, during each Monte Carlo step (MCS), the compositional evolution equations are solved 100 times. While $t < t + \Delta t$
   a) Solve the Cahn–Hilliard equation, Eq. 6, and globally update the vacancy composition
   b) Solve Eq. 9 and globally update the chemical composition
   c) Update time, $t = t + \Delta t_{\text{phase field}}$, where $\Delta t \gg \Delta t_{\text{phase field}}$

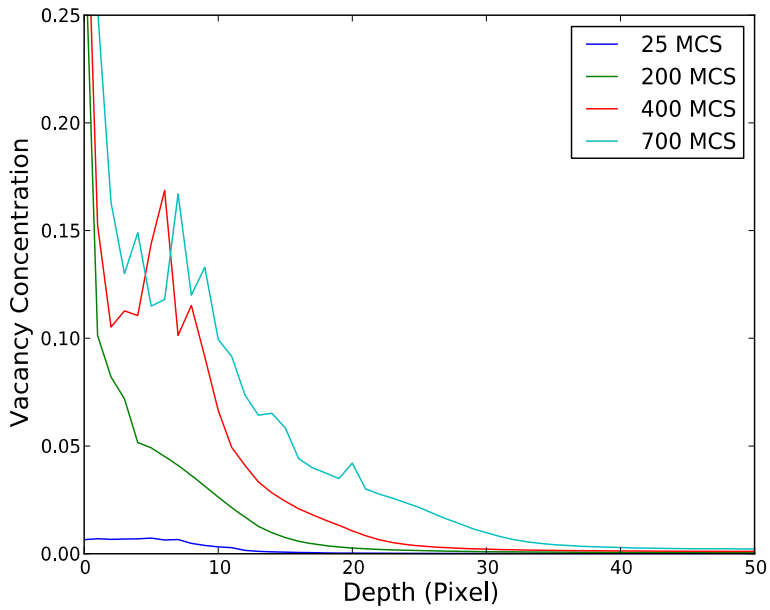

Figure 6: Vacancy concentration profile as it evolves with irradiation time.

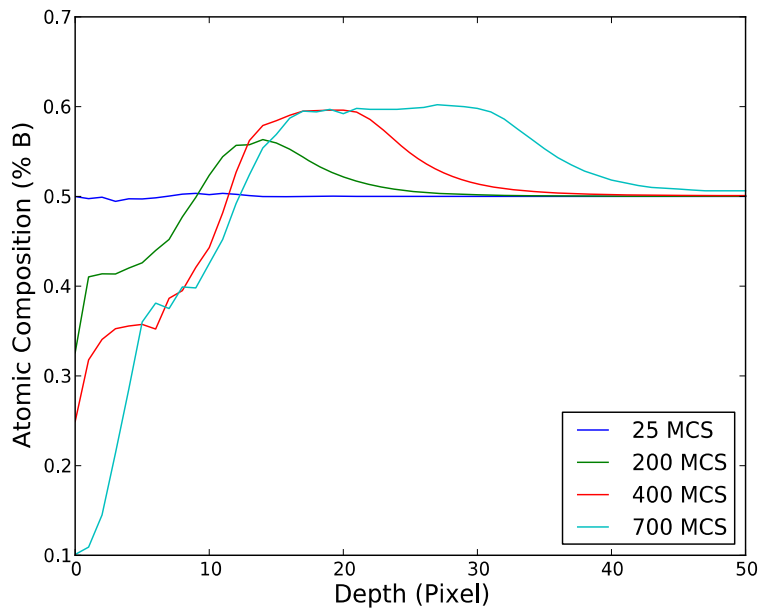

Figure 7: Chemical composition profile as it evolves with irradiation time.

5.1.2 Results and Discussion

As the material is irradiated, the vacancy concentration increases through the sample depth as shown in Figure 6. It increases at the surface at a faster rate than deeper into the target. This, in spite, of the fact that irradiation introduced more vacancies sub–surface than at the surface. This is a clear indication that vacancies are diffusing into the free surface, the only available sink. The vacancy profiles in Figure 6 are the average concentrations at that depth; the noise in the plots is due to roughening of the target

surface by surface diffusion. Thus, as the surface roughness increases, so does the noise in the data reported in Figure 6.

The B–component concentration profiles as a function of target depth z at different irradiation times are plotted in Figure. 7. The starting concentration of B is $C_B = 0.5$, but is depleted at the surface and enriched at increasing depths z with irradiation time. Since the diffusion of B through the vacancy mechanism is faster than that for A (i.e. $D_B^v > D_A^v$), B is depleted near the surface where the vacancy concentrations are high. This is due to the fact that the movement of a vacancy is directly correlated to the movement of an atom in the opposite direction, as evident from Eq. 8.

Chemical segregation is evident in Figure 8 which shows the composition and phase evolution. As irradiation proceeds and irradiation damage accumulates, the region closest to the surface starts to become enriched in A while the region just below becomes B–rich. As previously explained, this is because of the difference in diffusivities. Another interesting result is the phase transformation shown in Figure 8. As described in the Section *Phase Transformations*, when the chemical composition deviates considerably from the stoichiometric composition the material undergoes a phase transition. Once sufficient damage has been accumulated to create a stable A– or B–rich phase region, it can start nucleating and coalescing into a larger stable region.

5.1.3 Summary

One of the major advantages that this model provides is the coupling between composition and phase fields efficiently. Using the hybrid model we were able to accurately model the chemical segregation of an irradiated binary system. We show that even with the implementation of a single radiation–induced point defect type, the difference between diffusivities for each chemical component is sufficient to lead to segregation. Furthermore, it was shown that our model is able to simulate direct phase transformation due to compositional changes in the microstructure. From our results, we can contemplate that the depletion of As near the surface observed on Ga^+ irradiated $GaAs$, *Wei*[10], is possibly not solely a result of preferential sputtering. It is possible that the diffusion mechanism is the controlling process, which leads to the near surface segregation, as suggested by *Madi* for the surface nano–structuring case. Lastly, we see that this type of hybrid model that incorporates different processes into the evolution of a microstructure has great potential to simulate a wide range of complicated physics processes.

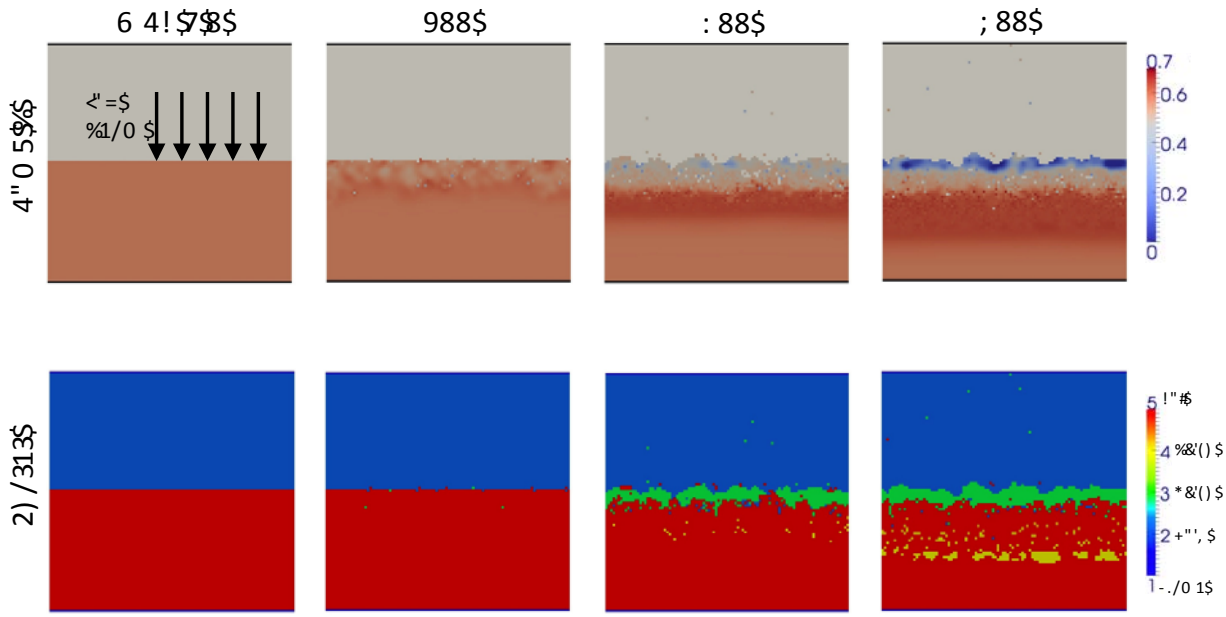

Figure 8: Evolution of the compositional and phase fields as the material is irradiated from the top. The creation and diffusion of the vacancies leads to chemical segregation and phase transformations.

5.2 Hybrid Model with Chemical Potential Driving Composition Evolution

The previous approach uses a concentration gradient driving force to evolve the microstructure. In order to have a proper thermodynamic description of the component segregation and phase transformation in this multi-phase system, the chemical potential must be used as the driving force, so Eq (14) becomes

$$\frac{\partial C_B}{\partial \tilde{t}} = \tilde{\nabla} \cdot \left(\tilde{D}_B \tilde{\nabla} \mu_B - \tilde{D}_v^B \tilde{\nabla} \mu_v\right). \tag{18}$$

to properly evolve the microstructure by leading the system to a thermodynamic equilibrium.

Phase-field models use the simplified definition of chemical potential, $\mu = df/dc$, as they use a continuous function for free energy f with minima corresponding to the stable phases and compositions. However, simulation of the binary GaAs with different free energy curves for each phase and irradiation defect energy corresponding to the density of irradiation defects, the full definition of chemical potential is required. In this section, the implementation of the complete chemical potential is described and the results of these simulations are shown.

5.2.1 Chemical Potential Definition

When using the simplified definition of the chemical potential, our model presented very unstable solutions to the microstructural evolution. Therefore, we have extended the definition of the chemical potential to a case where two phases are in equilibrium, as defined by the *Common Tangent Construction*[17], shown in Figure 9. This approach defines the chemical potential as

$$\mu_B = f_B + (1 - C_B) \cdot \frac{\partial f_B}{\partial C_B} \tag{19}$$

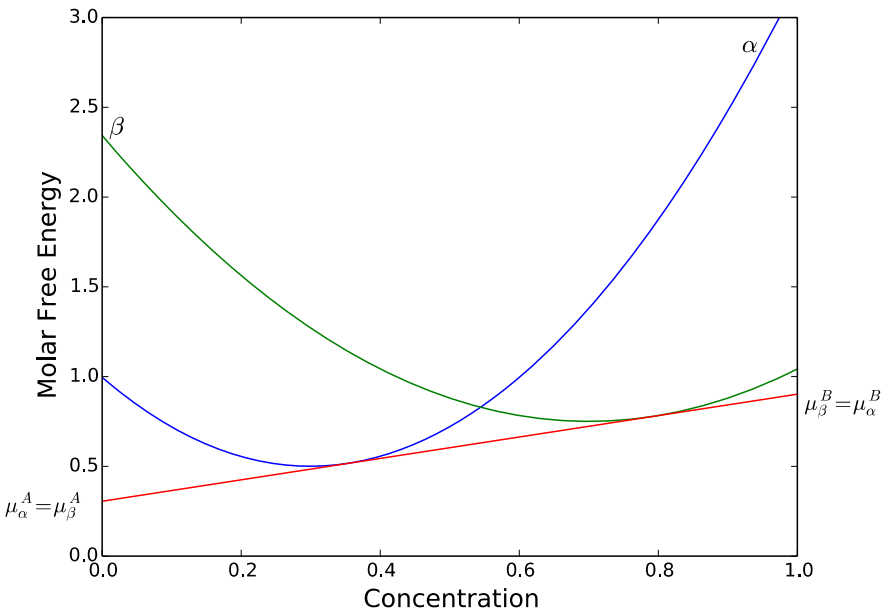

Figure 9. Graphical representation of the chemical potential as defined by the Method of Intercepts–Common Tangent Construction approach.

where f is the sum of the chemical free energy $\left(f_B^{bulk}\right)$ and the interfacial energy (E_{int}). This approach enables us to properly describe the microstructural evolution where the two phases move towards equilibrium, especially in the phase interfaces.

It should be noted, that to the best of our knowledge, this is the first time that this description has been used to define the chemical potential in a phase field problem.

5.2.2 Results and Discussion

To test the model, we simulate a stoichiometric initially single grain and phase $(\alpha\beta)$ material being irradiated with a distribution peaking close to the center of the material. Similar to the previous model, as we generate a vacancy concentration distribution, the differential vacancy diffusivity leads to chemical segregation. As shown in Figure 10, initially we get enrichment of component A around the radiation distribution peaking region. Eventually, as A is enriched, nucleation of the α −phase is achieved. Due to periodic boundary conditions and a uniform segregation induced enrichment of A along the horizontal direction, this phase grows quickly. This in turn, leads to an enrichment of B at the α −phase interface since the B component is being driven away from the nucleated phase. Eventually, we see nucleation of the β −phase, which is driven to a higher concentration, i.e. B enrichment.

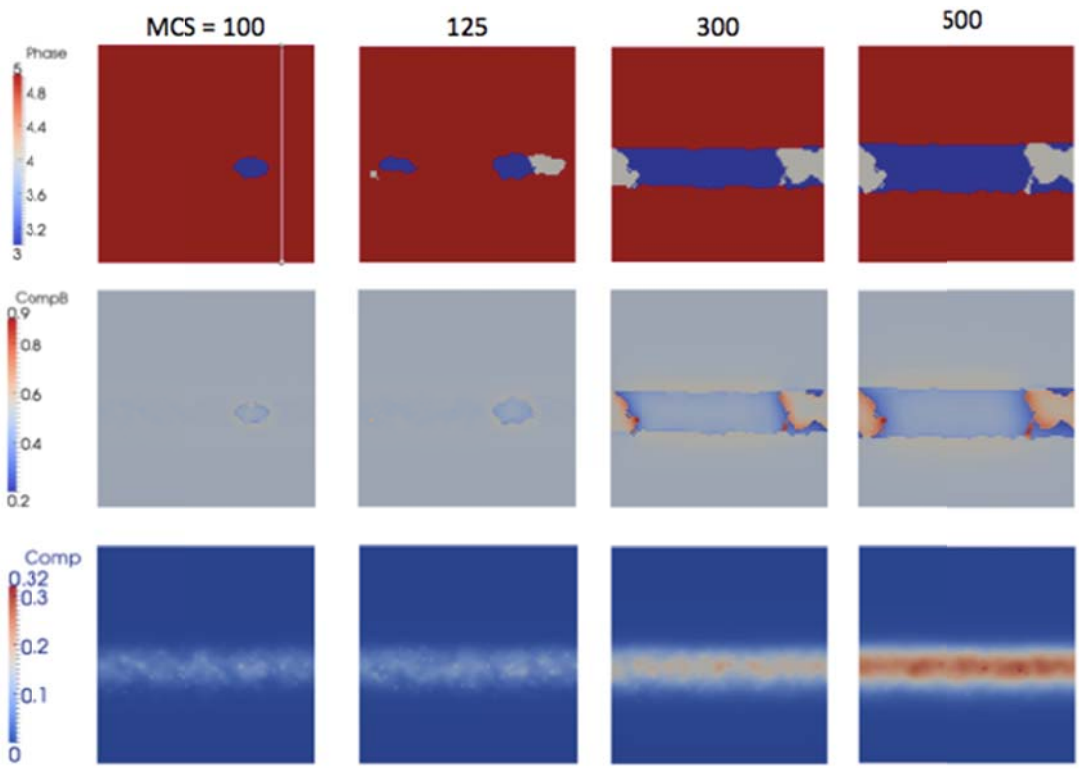

Figure 10: Evolution of the chemical and vacancy compositional, and phase fields as the material with a distribution peaking at the center. The creation and diffusion of the vacancies leads to chemical segregation and phase transformations; where red is the AB phase, blue is the $\boldsymbol{\alpha}$ phase and white is the $\boldsymbol{\beta}$ phase.

An interesting feature is the enhanced segregation along the phase interfaces, as evidence in Figure 10. We measure the concentration distribution evolution along two different lines through the simulation in Figure 10: Along one line, a single phase nucleates and grows, Fig.ure 11(b). Along the other line two phases phase nucleate and grow, Figure 11(a). The vacancy concentration profiles for both cases are very similar as would be expected, however, the B-concentration profiles are different. Initially, the two paths follow a similar compositional evolution with components A and B segregating similarly until nucleation starts taking place. After 125 MCS, we start seeing an obvious deviation between the compositon evolutions. For the two-phase case, Figure 11(a), several concentration "sinks" at the $\alpha - \beta$ interface start forming where each peak corresponds to the equilibrium concentration for the respective phases. For clarity purposes, let us look at the C_B distribution at 125 MCS. Going along the path from top (left) to bottom (right), we see the following features:

- Slight increase in the concentration: this is due to the α phase moving to a lower concentration
- Sharp decrease: boundary of the nucleated α phase at the equilibrium concentration
- Sharp increase: boundary of the nucleated β phase at the equilibrium concentration
- Gradual decrease/increase: bulk of the β phase slowly moves to the equilibrium concentration. The flux within the nucleated phase is much slower than at the interface

The single-phase B-concentration evolution shows peaks corresponding the α equilibrium concentration along the interface with the initially stable AB phase. This is a much simpler distribution, but with similar behavior of reaching the equilibrium concentration almost immediately after nucleation and a slower transition within the bulk of the phase. We should note that the concentration at the interfaces reaches equilibrium at a much faster rate than within the phase's bulk due to the larger difference in the chemical potential between different phases, i.e., larger driving force leads to a faster flux ($J \propto F \propto \nabla\mu$).

5.2.3 Summary

The use of the "complete" chemical potential definition leads to a more stable and thermodynamically accurate description of the microstructural evolution. This model was able to simulate a chemical depletion/enrichment behavior leading the nucleation and growth of distinct phases. As before, by simply allowing the vacancy differential diffusivity to drive the segregation, we are able to achieve nucleation of a complex multi-phased system.

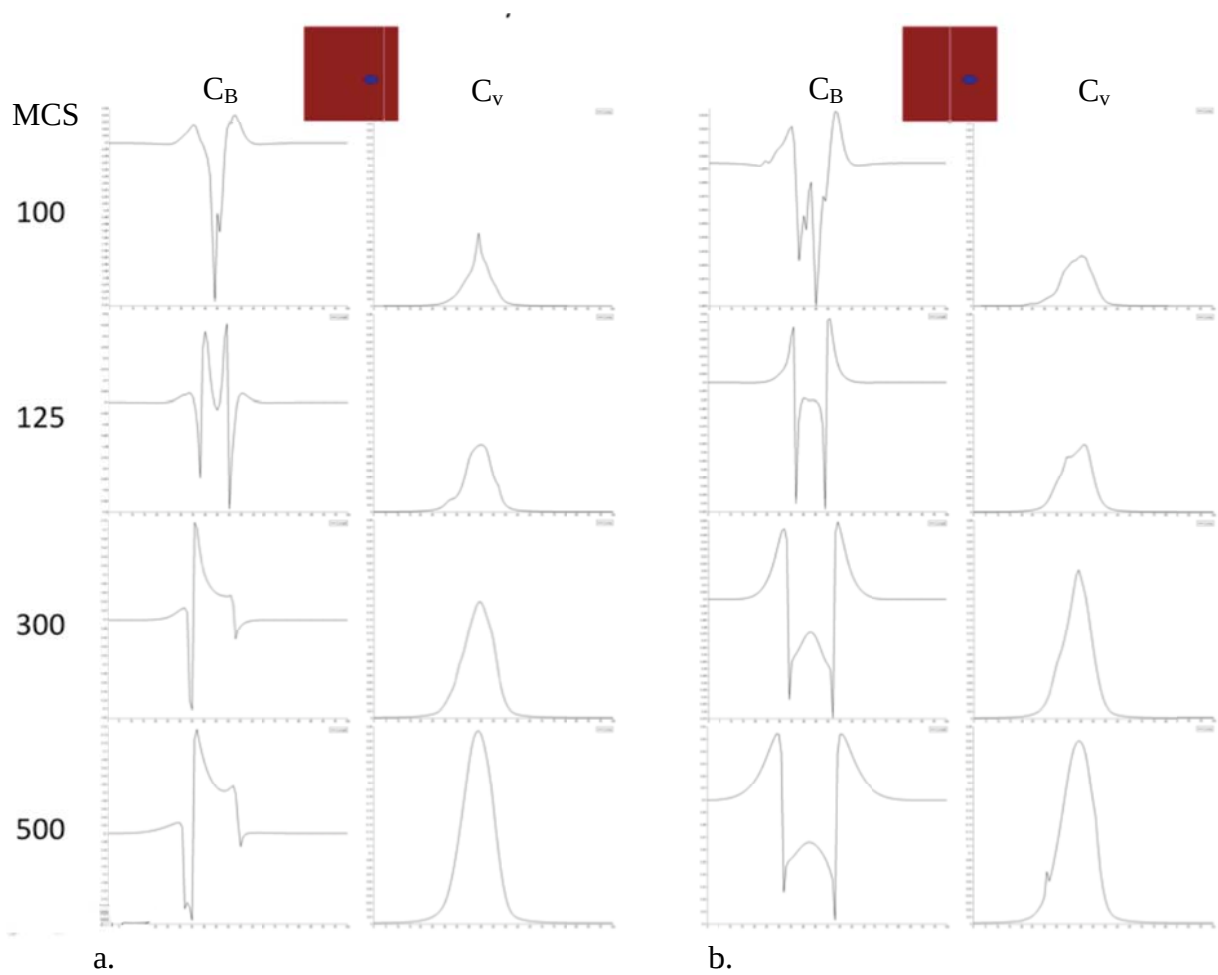

Figure 11: Chemical and vacancy concentration distribution along two different paths (inserts). We look at the concentration evolution along paths that include: a. nucleation of two phases, α and β. and b. nucleation of a single phase, α,

[1] P.R. Okamoto, L.E. Rehn, *Radiation–induced segregation in binary and ternary alloys*, J. Nucl. Mats. 83 (1979) 2–23.
[2] H. Wiedersich, P.R. Okamoto, N.Q. Lam, *A Theory of Radiation–Induced Segregation in Concentrated Alloys*, J. Nucl. Mats. 83 (1979) 98–108.
[3] S.M. Bruemmer, E.P. Simonen, P.M. Scott, P.L. Andresen, G.S. Was, L.J. Nelson, *Radiation–induced material changes and susceptibility to intergranular failure of light–water–reactor core internals*, J. Nucl. Mats. 274 (1999) 299–314.
[4] S. Le Roy, E. Barthel, N. Brun, A. Lelarge, S. Sondergard, *Self–sustained etch masking: A general concept to initiate the formation of nanopatterns during ion erosion*, J. Appl. Phys. 106 (2009) 094308 1–5.
[5] A.G. Perez–Bergquist, K. Sun, L. Wang, Y. Zhang, *Formation of GaSb core–shell nanofibers by a thermally induced phase decomposition process*, J. Mats. Res. 24 (2009) 2286–2292.
[6] G. Was, *Fundamentals of Radiation Materials Science: Metals and Alloys*, first ed., Springer, New York 2007.
[7] R.M. Bradley, J.M.E. Harper, *Theory of ripple topography induced by ion bombardment*, J. Vac. Sci. Technol. A 6 (1988) 2390–2395.
[8] A.G. Perez–Bergquist, K.D. Li, Y. Zhang, L. Wang, *Ion irradiation–induced bimodal surface morphology changes in InSb*, Nanotech. 21 (2010) 325602 1–6.
[9] Q. Wei, J. Lian, L.A. Boatner, L. Wang, R.C. Ewing, *Propagation of ripples on pyrochlore induced by ion beam bombardment*, Phys. Rev. B 80 (2009) 085413 1–8.
[10] Q. Wei, J. Lian, W. Lu, L. Wang, *Highly Ordered Ga Nanodroplets on a GaAs Surface Formed by a Focused Ion Beam*, Phys. Rev. Lett. 100 (2008) 076103 1–4.
[11] C.S. Madi, E. Anzenberg, K.F. Ludwig, Jr., M.J. Aziz, *Mass Redistribution Causes the Structural Richness of Ion–Irradiated Surfaces*, Phys. Rev. Lett. 106 (2011) 066101 1–4.
[12] J. Dabrowski, *Point Defect Assisted Diffusion in Semiconductors*, Sol. State Phen. 71 (2000) 23–50.
[13] E.R. Homer, V. Tikare, E.A. Holm, *Hybrid Potts–phase field model for coupled microstructural–compositional evolution*, Compt. Mat. Sci. 69 (2013) 414–423.
[14] J. Ziegler, M. Ziegler, J. Biersack, *SRIM: The Stopping and Range of Ions in Matter*, version 2008.03, LuLu, Morrisville NC (2008).
[15] G. Hobler, A. Simionescu, L. Palmetshofer, C. Tain, G. Stingeder, *Boron channeling implantations in silicon: Modeling of electronic stopping and damage accumulation*, J. Appl. Phys. 77 (1995) 3697–3703.
[16] E.A. Holm, C.C. Battaile, *The Computer Simulation of Microstructural Evolution*, JOM 53 (2001) 20–23.
[17] C.H.P. Lupis, *Chemical Thermodynamic of Materials*, first ed., Elsevier Science, New York 1983.

6. HYBRID POTTS-PHASE FIELD MODEL FOR COMPONENT SEGREGATION AND PHASE TRANSFORMATION IN U-PU-ZR FUELS

6.1 Introduction

The thermal and mechanical properties of materials, and their alloys, are strongly dependent upon the microstructure and phase of the material, both of which are effected by the material's composition. Environmental influences, such as a thermal gradient, can cause the constituents of an alloy to migrate, thus altering the local composition. Compositional changes can, in turn, alter the phase, microstructure and, ultimately, the material properties. This material property alteration, due to a redistribution of constituents under a thermal gradient, is observed in the metallic alloy U-Pu-Z.

U-Pu-Zr is a candidate fuel for advanced fast reactors because of its superior properties for high burnup, thermal response and inherent safety[1]. While limited characterization and performance data is available for the performance of systems of this particular alloy, it is clear that three concentric zones form when U-Pu-Zr is irradiated or subject to a thermal gradient[2,3]. These zones are compositionally and microstructurally inhomogeneous. This inhomogeneity alters the fuel behavior and performance, in that it causes phase transformations, solidus temperature changes and changes in the fissile atom density. Due to the expense, and to reduce the production of hazardous irradiated nuclear fuel, computational methods, utilizing the available U-Pu-Zr data, are used to model the evolution of such alloys.

While it is common in practice to model the microstructural and phase fields individually, these phenomena are actually interrelated. This is because the microstructure, which is often characterized by grains, grain boundaries and grain orientations, is dependent on local composition. Modeling the microstructural and phase-field evolutions together becomes increasingly important in multi-phase materials. A recently developed hybrid method, the Potts-phase field method, efficiently and effectively couples these two evolutions[4] and is extended to include three components, three phases and a thermal gradient. The objective of this research will be to apply the hybrid Potts-phase field method to model the microstructural, compositional and temperature profile evolutions of the U-Pu-Zr alloy.

6.1.1 Background

Metal fuels in nuclear reactors are advantageous because of their high thermal conductivity, ease of fabrication, high fissile and fertile atom density capability and theoretical increase in safety [5]. On the other hand, metal fuels cannot survive the high temperatures seen when using oxide fuels and, therefore, must operate at lower temperatures. The decreased operation temperature increases the fuel and reactor safety because it limits the diffusion of fusion gas bubbles, containing them within the fuel grains, and allows for a larger margin to overheating failure. U-Pu-Zr is a metal fuel of interest because of its high thermal conductivity which may make in inherently safe and its potential to provide long term management of plutonium[6].

The U-Pu-Zr alloy was originally explored as a fuel for the Experimental Breeder Reactor-II in the 60's, 70's and 80's, and was one of the alloys tested for the Integral Fast Reactor concepts, which began operation in February of 1985[3,7]. The fast reactors were developed to reach higher levels of fuel burn-up, and thus obtain more thermal energy out of the fuel. The nuclear fission process generates large temperature gradients from the core to the surface of the fuel. This thermal gradient drives phase changes enabled by constituent redistribution throughout the fuel rod.

A cross sectional optical photomicrograph of a post irradiated U-Pu-Zr fuel rod can be seen in Figure 12, showing the three concentric zones formed. While metallic fuels have the potential for the highest fissile atom density, i.e., the most heat/power generation, the resulting inhomogeneity in U-Pu-Zr alters the achieved fissile atom density and thus the fuel behavior and performance [8]. Fuel performance and life cycle times are influenced by this constituent redistribution but the greater problem affecting all nuclear fuels is the generation of fission gas bubbles that lead to porosity and loss of mechanical integrity. As a result of this loss of mechanical integrity, fuels are removed from service well before their theoretical burnup is achieved.

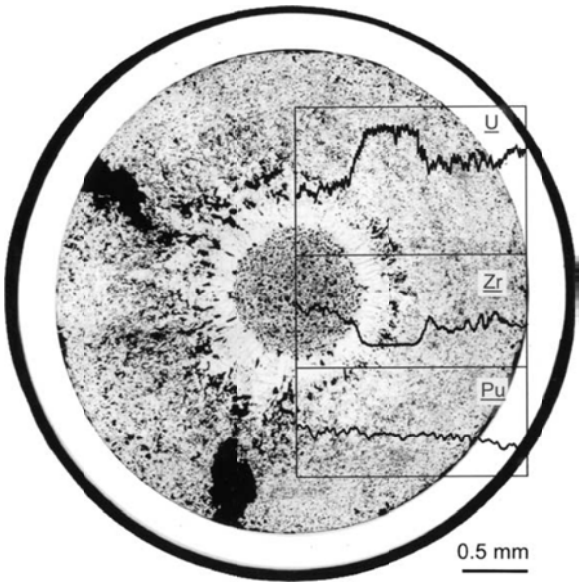

Figure 12. Micrograph of a U-Pu-Zr alloy, post-irradiation. Note the significant constituent redistribution driving the resulting concentric zones in the microstructure[8].

Previous work concerning fuels the U-Pu-Zr alloy have focused on modeling the distribution profiles via numerical methods, adjusting parameters to match experimental results. Ogawa and Iwai numerically solved a one-dimensional Fick's law and hypothesized the effect of including Pu in a U-Zr alloy, but did not compare model predictions to experimental data[9]. Ishida et al., extended the Marino model to the U-Pu-Zr system and, by assuming Pu was equally partitioned in U and Zr, defined the system as a quasi-binary system. The resulting model, however, predicted profiles that differed from experimental results and the errors were attributed to incorrectly predicting of temperature that were higher than anticipated[10]. Others have attempted to determine the kinetic values of the constituent diffusional coefficients and heat of transports via analytical models. Kim et al., investigated the kinetic and thermo-kinetic properties for irradiated U-Pu-Zr. They

calculated the interdiffusion fluxes from experimental test results and used the fluxes to then obtain the interdiffusion coefficients and heat of transport values. Later work by some of the same authors used a simplified pseudo-binary phase diagram, treating Pu to be immobile, to calculate the redistribution of Zr[11]. It is noted that while the use of binary or pseudo-binary systems, as done in the previous work, can yield approximate values, a true ternary modeling of the system should generate more accurate predictions to be able to investigate the effects of non-equilibrium constituent redistribution due to a thermal gradient.

The hybrid Potts-phase field method, which has been shown to accurately couple the microstructural and compositional evolutions of binary metallic alloys, can be extended to model ternary and higher order systems[12]. The method uses a Monte Carlo Potts model to evolve the microstructure, which is computationally efficient due to its ability to describe various features of the microstructure through single integer values. On the other hand, compositional evolution is modeled by the phase field method, which provides the necessary continuum variables that represent the state of the system at a given point [4]. This is possible through the use of kinetic equations, such as the Cahn-Hilliard Equation, which are dependent on the thermodynamics of the system, through the use of a free energy functional[13]. The coupled method has also demonstrated the ability to show thermal diffusion (the Soret Effect) and has allowed the incorporation of information made available through the use of thermodynamic databases[12].

In this work, we seek to create a more advanced model intended to simulate the response of U-Pu-Zr fuel in nuclear reactors. Fuels in fast nuclear reactors experience large thermal gradients, irradiation and pore generation and growth. The goal of this research will be to model the thermally driven redistribution of constituents in the U-Pu-Zr alloy and predict constituent redistribution profiles and concentric microstructures over a range of alloy compositions. The hybrid Potts-phase field method, has been expanded for a ternary system. The model is intended to provide a more accurate representation of the materials microstructural, compositional and temperature evolutions when in the presence of a thermal gradient. The effects of these evolutions on component segregation has been investigated. Ternary Gibbs free energy profiles, and the corresponding chemical potentials have been extracted from a thermodynamic database provided by Dr. M. Kurata[1].

6.2 Methodology

The Potts-phase field method[12] is extended to a ternary system with kinetic and thermodynamic values specific to the U-Pu-Zr alloy. In the hybrid Potts-phase field model, the composition of the system is evolved using Cahn-Hilliard approach

$$\frac{\partial C}{\partial t} = M\left[\nabla^2 f'(C) - \varepsilon \nabla^4 C\right] \tag{19}$$

where the chemical potential is defined as a function of the free energy functional, $f'=dF/dC$, and the concentration gradient. The Gibbs free energy can be characterized by an analytic function or, when incorporating data from a thermodynamic database, as the sum of the energies of the contributing phases.

Following the method outlined for a two-component system, we have determined the interdiffusion flux equations in a three-component system[12,15]. The flux equations, incorporating the diffusion of both mass and heat, are therefore determined to be

$$J_1 = -M_{11}\nabla(\mu_1 - \mu_3) - \frac{1}{2}(M_{33} - M_{11} - M_{22})\nabla(\mu_2 - \mu_3) - \frac{M_{1Q}}{T}\nabla T \tag{20}$$

$$J_2 = -\frac{1}{2}(M_{33} - M_{11} - M_{22})\nabla(\mu_1 - \mu_3) - M_{22}\nabla(\mu_2 - \mu_3) - \frac{M_{2Q}}{T}\nabla T \tag{21}$$

$$J_3 = \frac{1}{2}\left[M_{11}\nabla(\mu_1 - \mu_2) + M_{22}\nabla(\mu_2 - \mu_1) + M_{33}\nabla(\mu_1 + \mu_2 - 2\mu_3)\right] - \frac{M_{3Q}}{T}\nabla T \tag{22}$$

$$J_3 = \frac{1}{2}\left[M_{11}\nabla(\mu_1 - \mu_2) + M_{22}\nabla(\mu_2 - \mu_1) + M_{33}\nabla(\mu_1 + \mu_2 - 2\mu_3)\right] - \frac{M_{3Q}}{T}\nabla T \tag{23}$$

where J_1, J_2, J_3 and J_Q are the fluxes of the three constituents and the heat flux, respectively. It can be shown that $\sum_j M_{ij} = 0$ and $\sum_i M_{ij} = 0$ for network constraints.

In the ternary system we have used the full definition of the chemical potential as it is obtained from the free energy

$$\mu_1 = G\Big|_{C_2,C_3} - \frac{\partial G}{\partial C_2}\Big|_{C_2,C_3} C_2 - \frac{\partial G}{\partial C_3}\Big|_{C_2,C_3} C_3 \tag{24}$$

$$\mu_2 = G\Big|_{C_2,C_3} + (1 - C_2)\frac{\partial G}{\partial C_2}\Big|_{C_2,C_3} - \frac{\partial G}{\partial C_3}\Big|_{C_2,C_3} C_3 \tag{25}$$

$$\mu_3 = G\Big|_{C_2,C_3} + (1 - C_3)\frac{\partial G}{\partial C_3}\Big|_{C_2,C_3} - \frac{\partial G}{\partial C_2}\Big|_{C_2,C_3} C_2 \tag{26}$$

Beyond these extensions, the work largely follows previous work by Homer et al[4]. However, one of the primary challenges in accurately modeling the U-Pu-Zr has been the determination of the mobility constants, including the diffusional coefficients, heat of transports and other constants such as ε in Equation 19. Much of the needed data is largely missing so the best estimates of these values will be used.

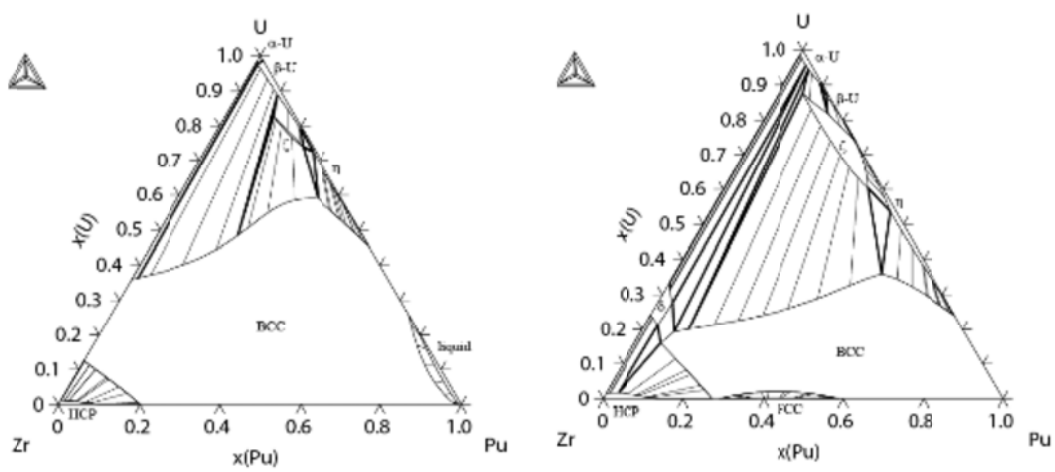

Figure 13. Phase diagram for the U-Pu-Zr system at 933 and 868 K, curtsey of Kurata.

The phase diagram for this system is shown in Figure 13. For the composition used in this work of U-25Zr-15Pu, the phases of interest are the bcc γ–phase that is stable at high temperatures and transforms to ζ– and δ– phases at lower temperatures.

6.3 Preliminary Results

The application of the Potts-phase field method to the U-Pu-Z system is still in its preliminary stages as validation exercises have not been completed. However the results are promising. Figure 14 shows results of a simulation starting with a composition of U-15Pu-25Zr with spins and phases assigned to each site at random in proportion to the composition. The temperature profile initially is a step function ranging from 950 to 700 K. s grains of a particular phase form, they grow to fill the local phase region. The γ–phase is the stable phase in the high temperature region as expected, with the ζ–phase becoming more stable at the intermediate temperatures and δ– phase being the stable phase at lower temperatures. The compositions of the three components diffuse to correspond to the components of their respective phases. And lastly the temperature smoothens to be consistent with the phase distributions seen in the simulations.

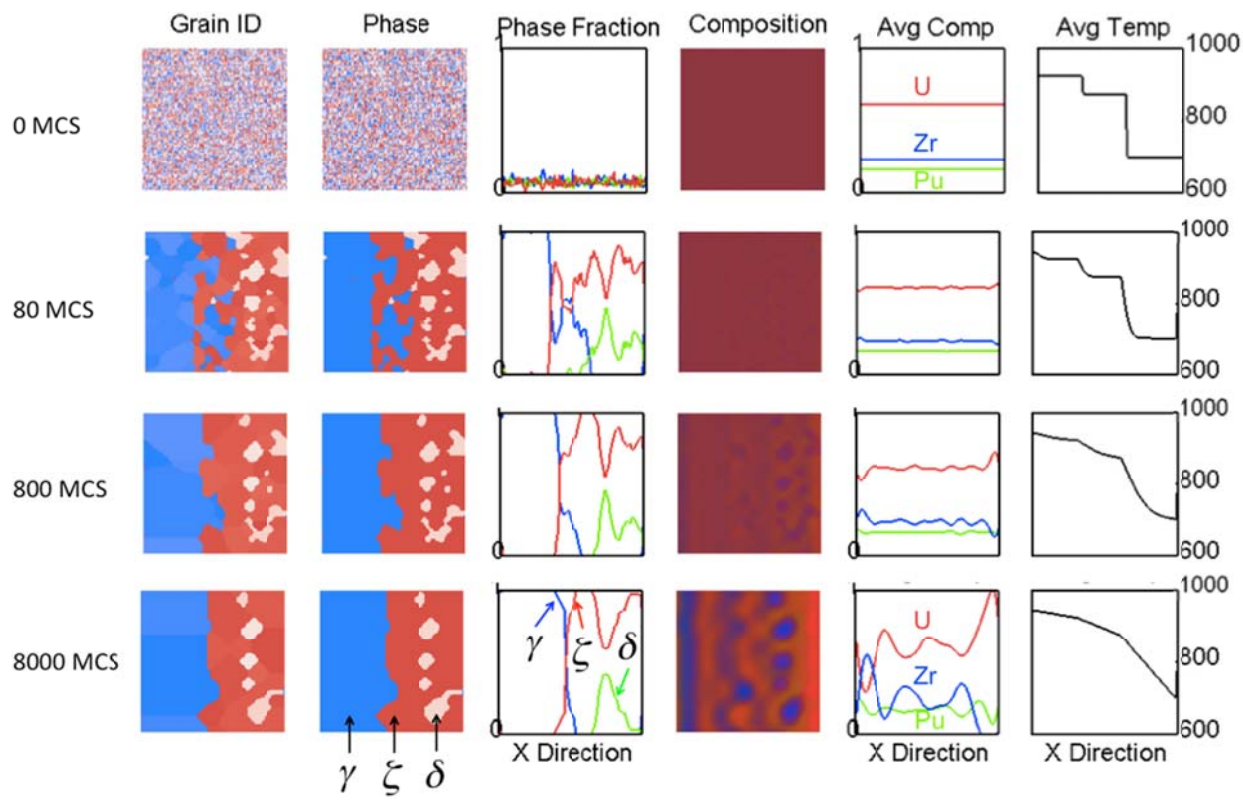

Figure 14. Simulation of U-25Zr-15Pu showing grain growth, phase nucleation and growth, phase and component segregation and evolving temperature profile.

---

[1] M Kurata. "Thermodynamic database on U-Pu-Zr-Np-Am-Fe alloy system I – Re-evaluation of U-Pu-Zr alloy system," *Materials Science and Engineering* 9 (2010) 012022.

[2] D. E. Burkes, J. R. Kennedy, T. Hartmann, C. A. Papesch, D. D. Keiser Jr., "Phase Characteristics of a number of U-Pu-Am-Np-Ar Metallic Alloys," *Journal of Nuclear Materials* 396 (2010) 49-56.

[3] W.F. Murphy, W.N. Beck, F.L. Brown, B. Koprowski, L.A. Neimark, "Postirradiation examination of U-Pu-Zr fuel elements irradiated in EBR-II to 4.5 atomic percent burnup," Argonne National Laboratory. *ANL-7602*, 1969.
[4] E.R. Homer, V. Tikare, E.A. Holm. "Hybrid Potts-Phase Field Model for Coupled Microstructural-Compositional Evolution." *Computational Materials Science*, 69 414–423 (2013).
[5] D. Mohr, L.K. Chang, E.E. Feldman, P.R. Betten, H.P. Planchon. *Nulcear Engineering Design* 101 (1) (1987) 45-56.
[6] State of the Union: The Advanced Energy Initiative. 2006.
[7] R.G. Pahl, D.L. Porter, C.E. Lahm, G.L. Hofman "Experimental Studies of U-Pu-Zr Fast Reactor Fuel Pins in the Experimental Breeder Reactor-II." July 1990.
[8] Y.S. Kim, G.L. Hofman, S.L. Hayes, Y.H. Sohn, "Constituent redistribution in U-Pu-Zr fuel during irradiation," *Journal of Nuclear Materials* 327 (2004) 27-36.
[9] G.P. Marino, *Nuclear Science Engineering* 49 (1972) 93.
[10] M. Ishida, T. Ogata, M. Kinoshita. *Nuclear Technology* 104 (1993) 37.
[11] Y.S. Kim, S.L. Hays, G.L. Hofman, A.M. Yacout, "Modeling of constituent redistribution in U-Pu-Zr metallic fuel," *Journal of Nuclear Materials* 359 (2006) 17-28.
[12] J.J. Cox, E.R. Homer, V. Tikare. "Hybrid Potts-phase field model for coupled microstructural-compositional evolution," *2012 Fall MRS Proceedings*, doi:10.1557/opl.2013.165.
[13] L. Zhang, M.R. Tonks, P.C. Millett, Y. Zhang, K. Chockalingam, B. Biner. "Phase-field modeling of temperature gradient driven pore migration coupling with thermal conduction," *Computational Materials Science* 56 (2012) 161-165.
[14] J.W. Cahn, J. Hilliard. *Journal of Chemical Physics* 28 (1958) 258.
[15] R. Balluffi, S. Allen, W.C. Carter. **Kinetics of Materials**, Hoboken: John Wiley & Sons; 2005.

7. DEVELOPMENT AND APPLICATION OF TOPOLOGICAL CHARACTERIZATION OF MICROSTRUCTURAL EVOLUTION

Topological characterization of 3D voxel-based images was developed in conjunction with NSF research grant DMR 1035188 on Topological Description of Grain Growth lead by Dr. Burton Patterson. Again, the work has been published in previous works and will only be summarized here. The reader is directed to the published works for detailed description of the topological characterization and it's application to studying grain growth.

Topological characterization of 3D voxel-based images is non-trivial. Since there are many scientific simulations that rely on digitized images consisting of voxel data, and usually need to be run in parallel, an accurate and efficient algorithm to characterize 3D microstructures in a cubic lattice is crucial for research on topology. We have developed an algorithm that enables detailed topological characterization that is extendible to parallel computing while retaining its efficiency and robustness. With this algorithm, a 3D microstructure made up of voxels can be accurately described in terms of faces, edges and vertices and the network formed by them. This algorithm is applied to various data sets consisting of idealized, regular structures and to microstructures generated by grain growth simulations. Highly accurate characterization of topology has been achieved for all data sets[1].

The topology and its changes were characterized using the topological characterization algorithm developed by following the topological evolution of individual grains during normal grain growth. These paths of evolution of topological grain forms during grain growth are described in terms of number of faces, edges per face and face arrangements, as depicted by Schlegel diagrams and the topological events that change them. This "Schlegel tree", Figure 15, describes transitions to higher face classes by grain encounters at corners and to lower face classes by grain-pair separation at three-edged faces. Transitions within face classes are described through rearrangements that occur to neighboring grains during these events. The process is further described by probabilities of the different paths in terms of numbers of edges, corners and three-edged faces at which face gain and loss events occur. Schlegel data from separated grains and three-dimensional Monte Carlo and front-tracking simulations show good comparison. Grain form frequencies increase with increasing number of transition paths into them from other forms. The highest frequency forms have few or no three-edged faces, while those with the most three-edged faces are present the least. These observations suggest that three-edged faces are catalysts for topological change, and forms with higher frequencies of these have shorter residence times before transitioning to lower classes[2].

Boundaries between neighboring grains with different numbers of faces exhibit a wide range of tendencies for occurrence in a structure, from high preference to high avoidance. By characterizing the topological evolution of individual grains, these tendencies for preference or avoidance are described here by their contact affinity, describing the extent by which an i-j faced grain-pair actually occurs in the structure relative to that expected from statistically random contact. An affinity of unity indicates random occurrence and values above or below unity indicate the corresponding factor above or below random that a particular pairing occurs. Grain contact affinities determined for both 3D Monte Carlo grain growth simulations and experimental serial sectioned grains show similar trends of

high affinity for contact between few- and many-faced grains, avoidance of contact between grains in similar face classes and random contact between grains of intermediate face classes and all other classes, Figure 16(a). Contact affinities have been modeled in terms of the relative face curvatures, with high curvatures of opposite sign exhibiting the highest contact affinities, like-signs the lowest, and relatively flat-faced grains showing near random contact with all other classes, Figure 16(b). The measure of affinity is thus interpreted as the degree of stability or instability of boundaries against rapid face loss from topological events. The affinity approach overcomes a significant bias of the Aboav-Weaire analysis that describes the average neighbors of face classes but is insensitive to the actual preference or avoidance for boundaries with other classes. The contact affinity term quantifies these tendencies[3]

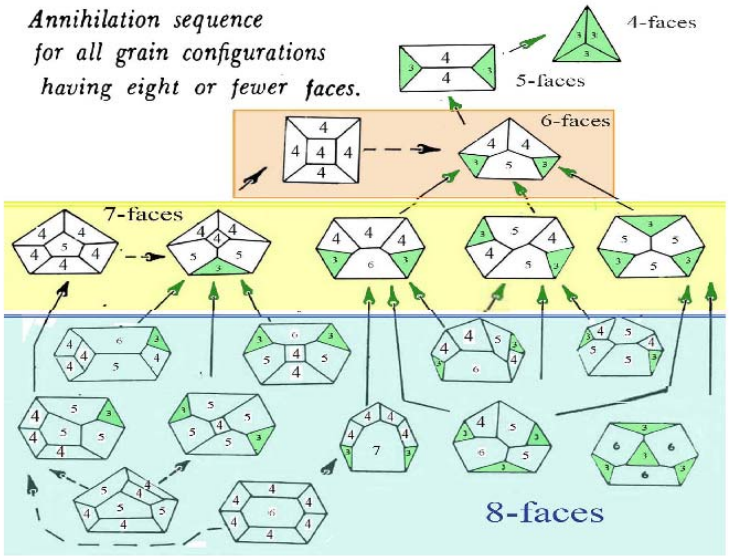

Figure 15. Steele's Schlegel tree illustrating grain forms in face classes 4 through 8. Solid arrows indicate paths of downward transition to the end state of a tetrahedron due to loss of particular 3-edged faces by Type I or III events. Dashed arrows indicate horizontal transitions within the face class, due to neighboring grains participating in Type II or III events.

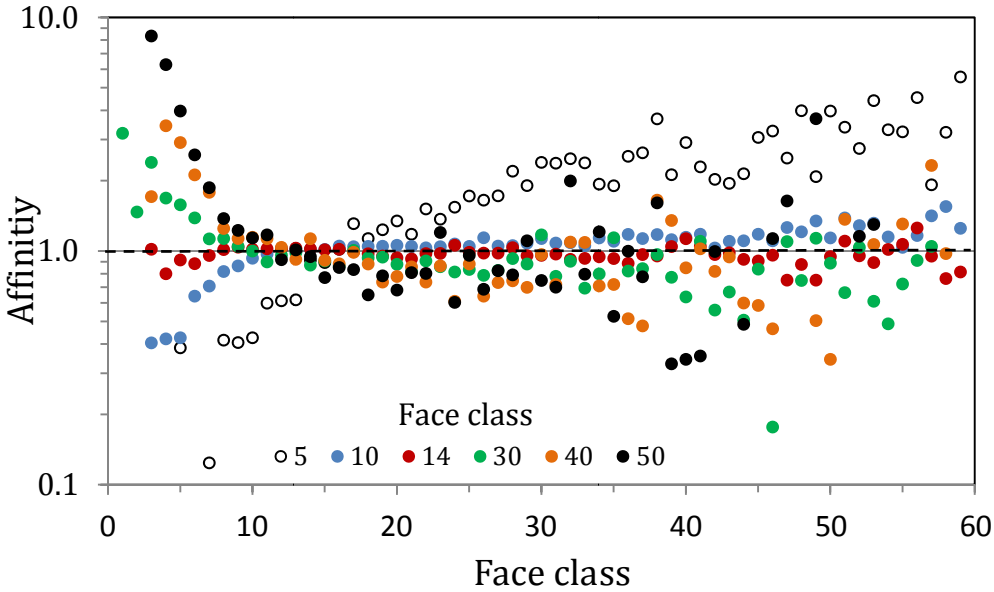

(a)

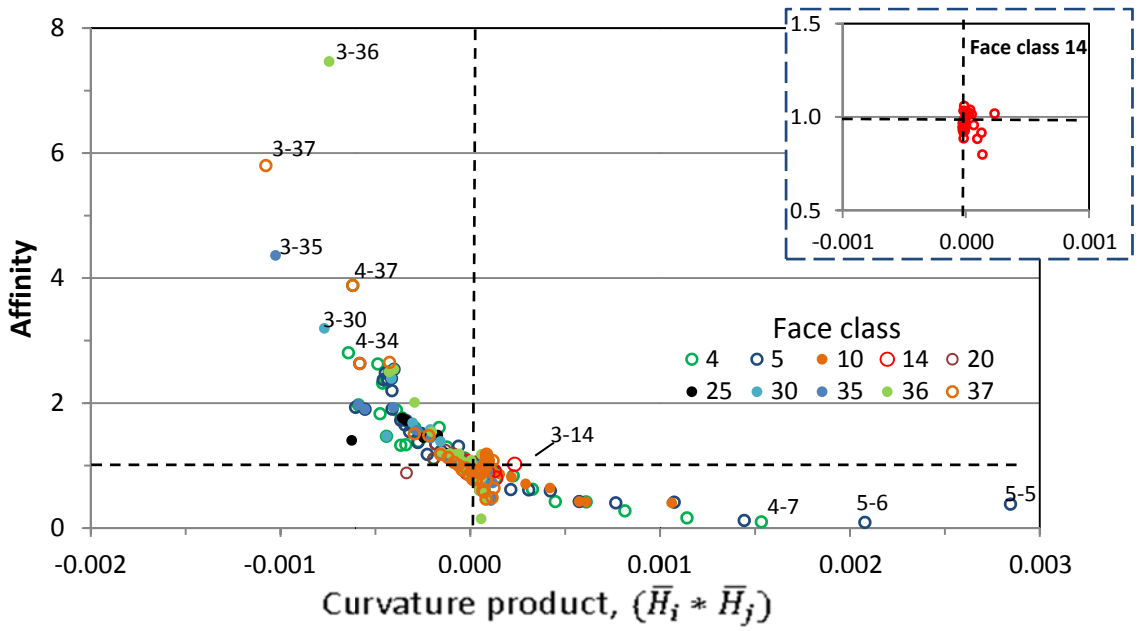

(b)

Figure 16. Contact affinity between grain pairs (a) of different face classes and (b) as a function of the product of face curvatures of the contacting grains.

---

[1] Z. Sun, V. Tikare, B. Patterson and A. Sprague, "Topological Characterization of Microstructure from 3D Digitized Voxel" *Comp. Mater. Sci.* 55 329-336 (2012).
[2] B.R. Patterson, D.J. Rule, R.T. DeHoff and V. Tikare, "Schlegel description of grain form evolution in grain growth", *Acta Mater.*, 61, 3986-4000 (2013).

[3] B.R. Patterson, D.J. Rowenhorst, V. Tikare, R.T. DeHoff and T.M. Kaub, "Affinities for Topological Arrangements in Grain Structures," accepted, *Acta Mater*.

8. A MOVING MESH PHASE-FIELD MODEL FOR MICROSTRUCTURAL EVOLUTION

8.1 Introduction

The recently-introduced moving mesh phase field model is applied to simulate grain growth. In this model, traditional phase field methods are applied on top of the computational framework of an adaptive moving mesh, greatly reducing the number of grid points needed for a simulation. We demonstrate the model for both bulk and thin film boundary conditions. Materials microstructures are structural or compositional heterogeneities found in a material, and they play an important role in determining material properties. Microstructure might consist of concentration heterogeneities, regions of different crystal orientations or phases, or domains of varying electric, elastic, or magnetic orientation. Understanding the temporal evolution of microstructure is often key to controlling the microstructure, and thereby, the properties of the material.

In the last 20 years, phase-field models have emerged as a popular way of studying microstructural evolution. The phase field model solves the evolution of one or more "order parameters", related to some physical property as concentration or grain orientation, and treats the order parameters as variables that change smoothly and continuously across interfaces between different regions. Treating the order parameters as continuous increases the numerical stability and speed of the numerical treatment, and allows us to avoid having to explicitly track the interfaces. Phase field modeling has been applied to many different types of materials and systems, including ferroelectrics[1,2], precipitation[3], Ostwald Ripening[4], and diffusion[5].

Microstructural evolution in phase field models is typically dominated by activity in the interfacial regions. In order to properly resolve and evolve these regions, the phase field model requires a minimum number of points across an interface, the number of which varies mildly between different computational methods. In systems where the interfacial area is small relative to the total simulation size, this resolution is the dominant limiting factor for simulation efficiency, as typically, the same resolution is applied everywhere. Large regions far from an interface may thus represent a large computational overhead, both in memory and speed, which is often unnecessary for accurate microstructural evolution.

Formerly, Feng and Chen[6] applied an adaptive mesh system to the Phase Field Model. In this formulation, the original orthogonal mesh underlying the numerical solution is allowed to deform smoothly over time, becoming a curvilinear grid with the same connectivity. Typically, the mesh is set to concentrate in regions where the gradient of the order parameter(s) is high, i.e., interfacial regions. This reduces the amount of total gridpoints needed for the evolution of the system, increasing computational efficiency. Here, we implement this computational tool, and we show its application to the evolution of a simple grain microstructure.

8.2 Theory

8.2.1 Description of the Computational Mesh and Its Movement

We desire a mapping between the computational domain, $\boldsymbol{\xi} = (\xi_1, \xi_2, \xi_3)$, and the physical domain, $\boldsymbol{x} = (x_1, x_2, x_3)$, such that the solution of a given physical order parameter, $u_i(\boldsymbol{x})$, is smoother and better-behaved in the computational space. To do this, we employ the variational formula:

$$I[\xi] = \int \sum_{i=1}^{3} \frac{\nabla_x \xi^i \cdot \nabla_x \xi^i}{\omega} dx. \tag{27}$$

where ω is called the "mesh monitor function" (MMF), and is related to the physical gradient of the order parameter by:

$$\omega = \sqrt{1 + \beta^2 |\nabla_x u|^2}. \tag{28}$$

We solve (1) as a time-dependent PDE, employing the gradient flow interpretation of the associated Euler-Lagrange. We also interchange the dependent and independent variables $\boldsymbol{\xi}$ and $\boldsymbol{x}$, to put the problem in a more convenient formulation. Thus, we arrive at a time-dependent PDE in terms of $\boldsymbol{x}(\boldsymbol{\xi})$, defining the temporal movement of the physical spacing of the mesh. Last, we apply a damping term γ to oscillations in the mesh movement, resulting in the semi-implicit mesh movement equation,

$$\left(1 - \gamma\, \nabla_\xi{}^2\right) \nabla x_i = -\, M_i \frac{\delta I[x_i]}{\delta x_i}, \tag{29}$$

where M_i is a kinetic parameter, related to the speed of the mesh movement. We solve the damped mesh movement equation via the Preconditioned Conjugate Gradient Method (for bulk) or the BiCGSTAB method (for films). For further detail, we reference the reader to Ref. [6-8].

We apply this moving mesh framework to systems with bulk boundaries (periodic along all three axes) and with film boundaries (periodic along x_1 and x_2; non-periodic along x_3). To determine the mesh at the boundaries for the film case, we set the x_3 locations of the mesh to be fixed along the boundaries (Dirichlet boundary conditions), while the x_1 and x_2 locations are free to move laterally along the boundary. For numerical stability reasons, we impose the Von Neumann boundary conditions on these latter two, setting $\frac{\partial x_1}{\partial \xi_3} = \frac{\partial x_2}{\partial \xi_3} = 0$.

Importantly, by including non-periodic boundary conditions, we can now consider effects such as (for example) a temperature gradient across the system, which can affect grain boundary mobilities or the bulk energy parameters. The non-periodic boundary conditions will also provide increased flexibility as we add other order parameters to this system in the future, such as concentration. To the authors' knowledge, this is the first time that non-periodic boundary conditions have been used with the moving mesh phase-field model.

8.2.2 Microstructural Evolution

We employ a simple, classic phase-field model for the evolution of grains[9], where different grains are distinguished by having a different dominant spin, η_i. I.e., we allow for q possible spins in the system, and in the interior of a grain, only one η_i will be non-zero. Interfacial regions are the regions between grains, where multiple spins are non-zero (typically, only

the spins of the grains neighboring the interface). With q available spins, the energy of the system is given as the following sum of the bulk (f_0) and gradient energies,

$$F[\eta] = \int \left(f_0\big(\eta_1(\boldsymbol{r}), \dots, \eta_q(\boldsymbol{r})\big) + \sum_{i=1}^{q} g_i (\nabla \eta_i(\boldsymbol{r}))^2 \right) d\boldsymbol{r}. \tag{30}$$

The bulk energy consists of a polynomial expression representing the local energy potential of a spin and its interaction with other (local) spins.

$$f_0 = \sum_{i=1}^{q} \alpha_i \, {\eta_i}^2 + \beta_i \, {\eta_i}^4 + \sum_{i=1}^{q} \sum_{j>i}^{q} \gamma_{ij} \, {\eta_i}^2 {\eta_j}^2 \tag{31}$$

Here, we employ normalized parameters for α_i and β_i such that there are $2q$ minima, 2 minima for each spin, at $\eta_i = \mp 1$. However, to maintain a consistent formulation, we set the values of the spins to their absolute value after a few timesteps, as the gradient energy contribution varies slightly between two grains of same-signed spins, versus two grains of opposite-signed spins. The term γ_{ij} describes the interaction between different spins.

We solve the temporal evolution of the system via the time-dependent Ginzburg-Landau equations for non-conserved parameters,

$$\frac{\partial \eta_i(\boldsymbol{r})}{\partial t} = -L_i \frac{\delta F(\eta)}{\delta \eta_i}, \quad (i = 1,2, \dots, q) \tag{32}$$

In order to increase the timestep of the simulation, we employ the semi-implicit formulation of (), solving the linear (gradient) term implicitly:

$$(1 - \Delta t \; g_i \; L_i \nabla^2) {\eta_i}^{n+1} = {\eta_i}^n - \Delta t \; L_i \frac{\delta f_0}{\delta {\eta_i}^n} \tag{33}$$

The semi-implicit solution is solved via the BiCGSTAB algorithm. We start the simulation from small random values for each spin, interspersed with smoothed, larger values, in order to represent a material nucleating and solidifying out of bulk.

Here, we employ the sum of the squares of all the spins as the function used in the mesh monitor function $u(\boldsymbol{x})$:

$$u(\boldsymbol{x}) = \sum_{i=1}^{q} {\eta_i}^2 \tag{34}$$

This also proves to be a useful function for visualizing the microstructural evolution, for the same reason: the values of $u(\boldsymbol{x})$ are 1 in the middle of a grain boundary, and somewhat less at the interface.

8.3 Results

We show here a simple proof-of-concept for a 2D microstructural evolution in a bulk system, grain growth in a 512 x 1 x 512 simulation space with periodic boundary conditions. The microstructure, mesh and a portion of the mesh is shown enlarged below. As one can see, the mesh is much more dense in the grain boundary regions where the mesh is much finer than in the grain interiors. This is also where the order parameter is changing, so computation should be more efficient in the overall simulation.

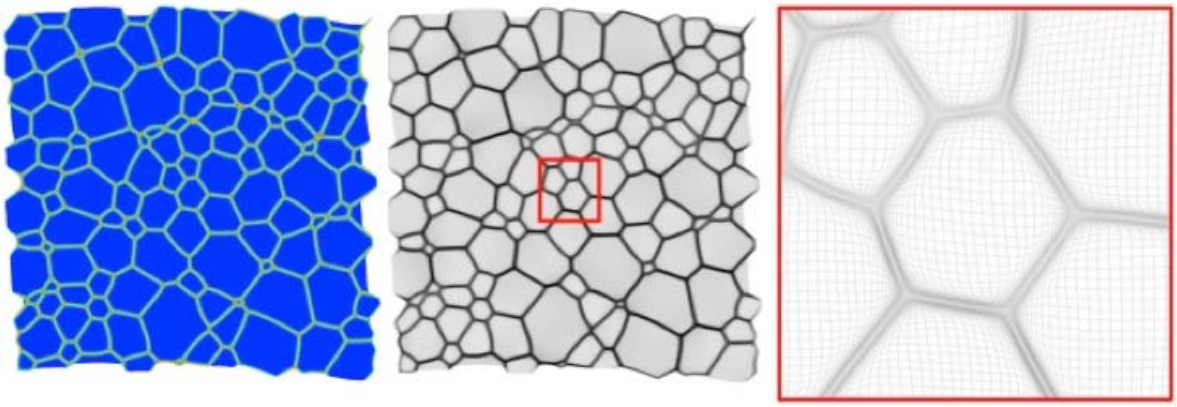

Figure 17. Simulation of grain growth using the moving mesh phase field model.

The moving mesh phase field model is also demonstrated on a thin film with periodic boundary conditions in the x-direction, but not the y-direction. Again the mesh is finest in the grain boundary regions where the order parameters are changing. The distortions due to the large grain traversing the simulation space are minimal.

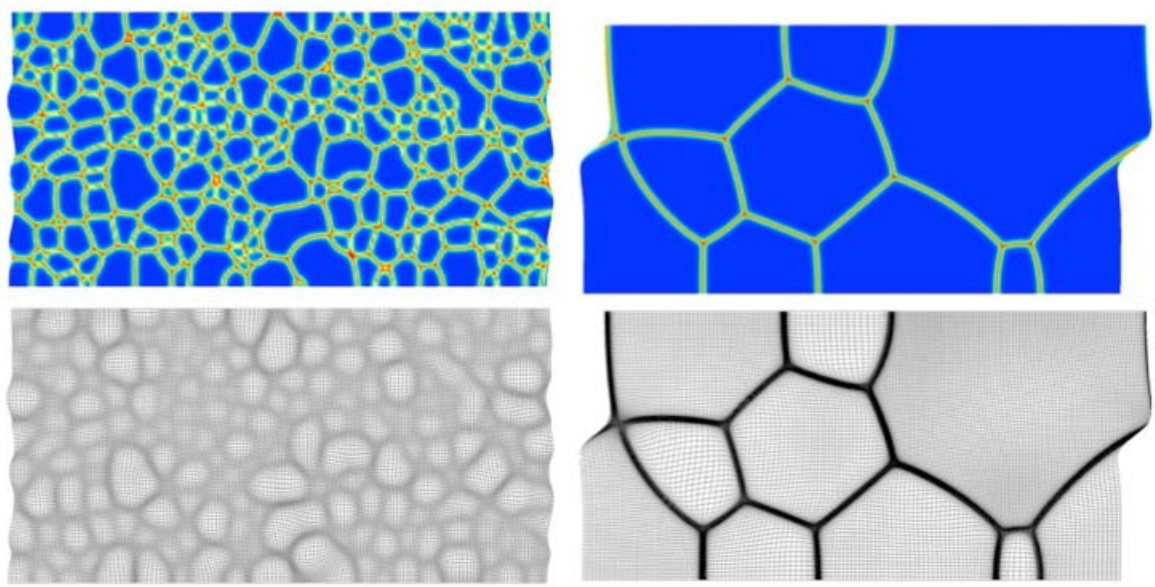

Figure 18. Simulation of grain growth in a thin film with large grains traversing the periodic boundary conditions in the x-direction. The distortion in the mesh do not distort the overall grain structure.

This new capability will allow more efficient simulation of phase-field models and hybrids that use this capability.

[1] F. Xue *et al*., *Acta Mat.*, **61** (2013) 2909-2918.
[2] Y. L. Li *et al*., *Acta Mat.*, **50** (2002) 395-411.
[3] X. Q. Ma *et al*., *Scripta Mat.*, **47** (2002), 237-241.
[4] D. N. Fan *et al*., *Acta Mat.*, **50** (2002), 1895-1907.
[5] J. H. Zhu *et al*., *Comp. Mat. Sci*., **20** (2001), 37-47.
[6] W.M. Feng *et al*., *J. Comp. Phys*., **220** (2006) 498-510.
[7] W. Huang, *J. Comp. Phys.*, **171** (2001) 753-775.
[8] W. Huang and R. Russell, *SIAM J. Sci. Comput.*, **20** (1999) 998-1015.
[9] C. E. Krill III and L.-Q. Chen, *Acta Mat.*, **50** (2002) 3057-3073.

Distribution

1 Elizabeth A. Holm, Ph.D.
Materials Science and Engineering
Carnegie Mellon University
5000 Forbes Avenue
Wean Hall 3301
Pittsburgh, PA 15213

2 Burton R. Patterson
Department of Materials Science and Engineering
University of Florida
PO Box 116400
223 Materials Engineering Bldg. (MAE)
Gainesville, FL 32611-6400

3 Eric R. Homer
Brigham Young University
Dept. of Mechanical Engineering
435 CTB
Provo, Utah 84602

MS0359	D. Chavez, LDRD Office	01911
MS0501	Jonathan Zimmerman	08256
MS0736	Dana Powers	06220
MS0744	Patrick Mattie	06233
MS0747	Ken B. Sorenson	06223
MS0747	Sylvia Saltzstein	06225
MS0747	Remi Dingreville	06233
MS0747	Veena Tikare	06225
MS0747	Efrain Hernandez-Rivera	06225
MS0751	Thomas Dewers	06914
MS0779	Carlos Jove-Colon	06222
MS0779	Yifeng Wang	06222
MS0840	Eliot Fang	01524
MS0840	John Pott	01525
MS0878	Allen Roach	02735
MS0878	Daniel Kammler	02735
MS0889	Corbett Battaile	01814
MS0889	S. Jill Glass	01818
MS1136	Gary Rochau	06221
MS1316	Steven Plimpton	01426
MS1320	Aidan Thompson	01426
MS1322	John Aidun	01425
MS1411	Amy Sun	01814
MS1411	Stephen Foiles	01814

MS1411	Paul Clem	01816
MS1411	Goeffrey Brennecka	01816
MS1415	Carlos Gutierrez	01114
MS1415	Tina Nenoff	01114
MS9957	Gregory Wagner	08365
MS0899	Technical Library	09536 (electronic copy)

Sandia National Laboratories